Neoarchean magmatism in the southern Scott and Raggatt Mountains, Napier Complex, east Antarctica

Precambrian Research xxx (xxxx) xxx

Contents lists available at ScienceDirect

Precambrian Research

journal homepage: www.elsevier.com/locate/precamres

Neoarchean magmatism in the southern Scott and Raggatt Mountains, Napier Complex, east Antarctica

Piotr Król [a,*], Monika A. Kusiak [b], Daniel J. Dunkley [b], Simon A. Wilde [c], Keewook Yi [d], Martin J. Whitehouse [e], Shinae Lee [d], Simon L. Harley [f]

[a] Institute of Geological Sciences, Polish Academy of Sciences, Warsaw, Poland
[b] Institute of Geophysics, Polish Academy of Sciences, Warsaw, Poland
[c] School of Earth and Planetary Sciences, Curtin University, Perth, Australia
[d] Korea Basic Science Institute (KBSI), Ochang Campus, Republic of Korea
[e] Department of Geosciences, Swedish Museum of Natural History, Stockholm, Sweden
[f] School of GeoSciences, University of Edinburgh, Edinburgh, UK

ARTICLE INFO

Keywords:
East Antarctica
Enderby Land
Napier Complex
Archean granitoids
Zircon
U-Pb geochronology

ABSTRACT

The Napier Complex of Enderby Land and Kemp Land is a unique part of the Eastern Antarctic Shield, as it preserves history of crustal growth extending from the Eo- to Neoarchean. It is composed mainly of enderbitic and charnockitic gneisses and granulites metamorphosed at *ca.* 2.5 Ga, and locally at *ca.* 2.8 Ga, under high- to ultra-high temperature conditions. These events have been well-characterized in the central and western parts of the complex; however, the south-southwestern region has been little studied. Samples from the southern Scott and Raggatt Mountains were selected for zircon U-Pb dating by Secondary Ion Mass Spectrometry and whole-rock geochemical analysis. Tonalitic gneiss from the Raggatt Mountains and trondhjemitic gneiss from the southern Scott Mountains have protolith ages of 2711 ± 5 Ma and 2726 ± 6 Ma, respectively. In contrast, tonalitic samples from the southern Scott Mountains have protolith ages of *ca.* 2539 ± 5, 2533 ± 5 and 2522 ± 9 Ma. The younger generation of magmatism overlaps the timing of metamorphic zircon growth between 2540 and 2440 Ma observed in this study. The geochemistry of *ca.* 2720 Ma gneisses indicates that magmatism was generated by medium-pressure melting (>1.5 GPa) of basaltic crust, whereas *ca.* 2530 Ma magmas were generated at lower pressures (<1.2 GPa). The *ca.* 2.7 Ga magmatism may be associated with continental crust formed at 2.8 Ga, or be newly formed crust that was assembled with older prior to or during a tectonometamorphic event at *ca.* 2.5 Ga. Tonalitic magmatism at 2.53 Ga during the first half of the 2585–2420 Ma metamorphic event may be a product of partial melting during high-grade metamorphism. Although protolith ages across the complex are still scarce, differences between regions raise the possibility that the complex contains crustal domains of different ages and origins that may not have been assembled until the *ca.* 2.5 Ga tectonothermal event.

1. Introduction

The Napier Complex of Enderby Land and Kemp Land has attracted considerable geological interest due to the preservation of some of the oldest remnants of Earth's continental crust (Sobotovich et al., 1976; Black et al., 1986b; Harley and Black, 1997; Kelly and Harley, 2005; Belyatsky et al., 2011; Kusiak et al., 2013a,b, 2021; Król et al., 2020). It has a complex late Archean geological history involving granulite facies metamorphism at *ca.* 2.84–2.80 Ga and long-lived high- to ultra-high temperature (UHT) granulite metamorphism at 2.59–2.42 Ga, respectively (Harley and Black, 1997; Clark et al., 2018). The latter tectonothermal episode resulted in some of the highest regional metamorphic temperatures recorded by crustal rocks (Ellis, 1980; Harley and Motoyoshi, 2000; Hokada et al., 2008; Harley et al., 2019 and references therein), with peak UHT temperatures estimated to have exceeded 1000 °C and even approached 1100 °C, at pressures of 0.7–1.1 GPa. Recent studies on the Napier Complex have mainly focused on deciphering the nature of the earliest crust (Hiess and Bennett, 2016; Guitreau et al., 2019; Król et al., 2020; Kusiak et al., 2021) and the timing and duration of the UHT metamorphic event (Mitchell and Harley, 2017;

* Corresponding author at: Institute of Geological Sciences, Polish Academy of Sciences, Twarda 51/55, 00-818 Warszawa, Poland.
E-mail address: piotr.krol@twarda.pan.pl (P. Król).

https://doi.org/10.1016/j.precamres.2021.106530
Received 4 June 2021; Received in revised form 16 December 2021; Accepted 17 December 2021

Clark et al., 2018).

The record of Archean crustal development and late Archean granulite to UHT metamorphism in the Napier Complex is principally documented in detail from localities that are widely spaced and, moreover, mainly located in the Tula Mountains and areas surrounding Amundsen Bay and Casey Bay in the west of the complex (Fig. 1). So far, very little geochronological work, and no systematic zircon U-Pb geochronology, has been conducted on the southernmost parts of the Napier Complex, specifically in the Raggatt and Scott Mountains that collectively cover an area of some 2500 km^2 to the east and southeast of Casey Bay, Fyfe Hills and Mount Cronus. This potentially presents a major gap in our understanding of the make-up of the Napier Complex, for example whether all of its post-3.0 Ga history is consistent over its entirety, or whether it is comprised of multiple Archean crustal blocks that were brought together in the late Archean. In order to address this knowledge gap, this study presents new Secondary Ion Mass Spectrometry (SIMS) U-Th-Pb geochronological data obtained on legacy samples of orthogneisses from the Raggatt and southernmost Scott Mountains (Fig. 1) that allow this region to be compared with previously dated areas. Zircon U-Pb results are combined with whole-rock geochemical analyses to evaluate the source of the protoliths, the depth of generation of protolith melts and their possible geotectonic settings, providing for a more integrated understanding of the Napier Complex.

2. Geological setting and geochronology

The Napier Complex extends along the Antarctic coast between longitudes 48°E and 57°E (Fig. 1). It is a part of the East Antarctic Shield, which records a prolonged history of continental growth and terrane assembly throughout the Proterozoic and into the Cambrian (Fitzsimons, 2000; Harley et al, 2013). The geology of the Napier Complex has been summarized by Sheraton et al. (1987) and more recently by Harley et al. (2019). The complex is composed mostly of gneisses and granulites formed under high temperature (HT) to UHT conditions at *ca.* 2.5 Ga (Clark et al., 2018; Harley et al., 2019, Lyon et al., 2019) and locally at *ca.* 2.8 Ga (Harley and Black, 1997; Clark et al., 2018; Król et al., 2020). Orthopyroxene-quartz-feldspar orthogneisses and layered garnet-quartz-feldspar paragneisses are the most common rock types, with minor mafic components. Orthogneisses range from tonalite (enderbite) through tonalite–trondhjemite–granodiorite (TTG) to granite (charnockite) in composition. The Scott and Raggatt Mountains (Fig. 1A) are inland mountain ranges located in the southwestern Napier Complex. The outcrops in this area are composed mainly of orthopyroxene-quartz-plagioclase gneisses, with less diversity of rock composition than is characteristic elsewhere in the complex (Sheraton et al., 1987; Król et al., 2020). Whereas mesoperthite-bearing charnockitic gneisses metamorphosed up to UHT conditions (Harley, 2016) are particularly abundant around Amundsen Bay and in the Tula Mountains, rocks with similar bulk compositions in the southern Scott and Raggatt Mountains typically contain plagioclase and orthoclase (Sheraton et al., 1987), probably reflective of lower peak metamorphic temperatures. Indeed, the southern Scott and Raggatt Mountain regions lie outside of the UHT metamorphic domain as outlined by Harley and Motoyoshi (2000) based on the geothermobarometry of garnet-orthopyroxene-bearing granulites (Harley, 1985) and characteristic mineral assemblages in pelites (Harley

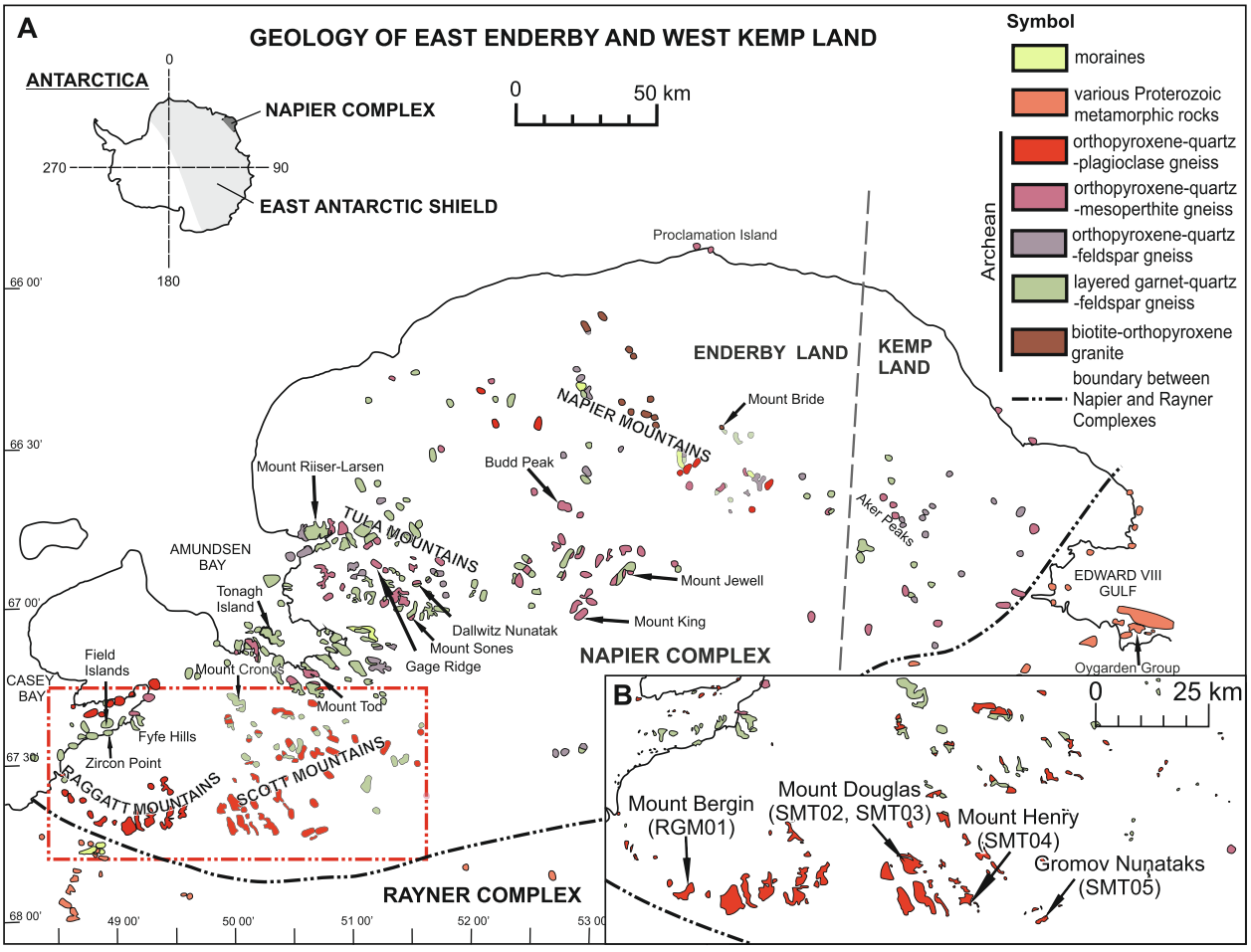

Fig. 1. Map of the Napier Complex, modified after Sheraton et al. (1987). A – Simplified outcrop map. Study area is marked by the dashed red rectangle. Inset shows the position of the Napier Complex within the East Antarctic Shield. B – Outcrop map of the Raggatt and southern Scott Mountains. Sample locations are indicated.

et al., 1990 and references therein). There is no reason to propose that the granulites of this region ever experienced the UHT conditions recorded to the north and northwest.

The crust in the Napier Complex formed throughout most of the Archean. Eoarchean protoliths for felsic orthogneisses are known from zircon dating at several localities in the Tula Mountains, *i.e.,* Mount Sones (Guitreau et al., 2019), Gage Ridge (Kusiak et al., 2013a; Guitreau et al., 2019), Budd Peak and Mt. Jewell (Król et al., 2020). Eoarchean crustal formation was also confirmed in one isolated locality at Aker Peaks in Kemp Land (Kusiak et al., 2021), 200 km to the east. Protolith ages for felsic orthogneisses at Mt. Riiser-Larsen vary from 3267 ± 5 to 3073 ± 12 Ma (Hokada et al., 2003). Elsewhere, zircon U-Pb ages between 2988 ± 23 and 2837 ± 15 Ma have been reported from several localities in the central and northern Napier Complex (Harley and Black, 1997; Kelly and Harley, 2005; Król et al., 2020). Additionally, Rb-Sr whole-rock ages may indicate protolith formation at that time, including: 3120 $^{+230}/_{-180}$ Ma at Fyfe Hills, 2934 $^{+196}/_{-127}$ Ma at Mount Tod in Amundsen Bay (Black et al., 1983b), and 2840 $^{+220}/_{-280}$ Ma at Mount Bride in the Napier Mountains (Black et al., 1986a). Variation in protolith ages between different localities is reflected by neodymium depleted mantle ($Nd(t)_{DM}$) model ages (3950–3030 Ma, recalculated from previous studies by Shiraishi et al., 2008).

The Napier Complex was locally affected by a tectonothermal event at *ca.* 2.8 Ga as demonstrated by several authors (*e.g.,* Harley and Black, 1997; Kelly and Harley, 2005; Kusiak et al., 2013a; Clark et al., 2018; Król et al., 2020). *Circa* 2850 Ma ages for metamorphic zircon were obtained for gneisses from Mt. Riiser-Larsen (Hokada et al., 2003), Dallwitz Nunatak (Kelly and Harley, 2005; Kusiak et al., 2013a) and Proclamation Island (Kelly and Harley, 2005). Król et al. (2020) provided a slightly younger estimate of *ca.* 2826 ± 10 Ma from a granitic gneiss from Mount King. However, Hokada et al. (2003) suggested, based on zircon dating, that this tectonothermal event continued at least until 2790 Ma. A magmatic age of 2788 ± 24 Ma has been obtained for a gneiss from Mt. King (Król et al., 2020). This, however, constitutes a minimum age and its relationship to the *ca.* 2.8 Ga metamorphic event remains unresolved. The only known protolith ages for orthogneisses that resolvably postdate *ca.* 2.8 Ga metamorphism are known from Fyfe Hills (*ca.* 2741 Ma, Horie et al., 2012) and Tonagh Island (2678 ± 8 Ma, Crowe et al., 2002; 2628 ± 12 Ma, Carson et al., 2002a).

Granulite to ultra-high temperature metamorphism between 2585 and 2420 Ma has been well-established by zircon and monazite dating (Grew and Manton, 1979; Asami et al., 2002; Carson et al., 2002a; Kelly and Harley, 2005; Suzuki et al., 2006; Horie et al., 2012; Harley, 2016; Clark et al., 2018; Król et al., 2020). The oldest estimate for this event was obtained from zircon growth in anatectic leucosome from McIntyre Island (2586 ± 8 Ma, Harley, 2016). Ages from metamorphic zircon between 2550 and 2520 Ma were obtained from Tonagh Island (Carson et al., 2002a), Zircon Point (Kelly and Harley, 2005), Fyfe Hills (Horie et al., 2012) and Mount King (Król et al., 2020). However, zircon growth and/or modification until 2450 Ma has been demonstrated in many studies (Black et al., 1983a; Carson et al., 2002a; Hokada et al., 2003; Kelly and Harley, 2005; Horie et al., 2012; Takehara et al., 2020; Kusiak et al., 2021). In some samples (*e.g.,* Kelly and Harley, 2005; Król et al., 2020) two distinct stages of metamorphic zircon growth have been identified with different Th-U compositions (*e.g.,* 2513 ± 8 and 2480 ± 6 Ma in granitic gneiss from Budd Peak (Król et al., 2020). Younger estimates from zircon, monazite and xenotime (Black et al., 1984; Asami et al., 2002) down to *ca.* 2420 Ma have been attributed to slow cooling and/or fluid activity (*e.g.,* Harley, 2016).

3. Methodology

For whole-rock analyses of major and trace elements, fresh and compositionally uniform samples were pulverized in an agate ball mill to ~200 mesh. Analyses were performed by Bureau Veritas Minerals at ACME Analytical Laboratories, Vancouver, Canada. Major oxides were analysed by X-ray fluorescence (XRF) spectrometry, whereas trace elements, including rare earth elements (REE), were analysed by inductively-coupled plasma mass spectrometry (ICP-MS). The volatile content was estimated by loss on ignition (LOI), measured by titration. Geochemical results are presented in diagrams created with the GeoChemical Data toolkit (GCDkit) for R, using the procedures of Janoušek et al. (2016). The results are compared with published data for other felsic orthogneisses in the Napier Complex (Sheraton et al., 1987; Król et al., 2020). They are also compared with data from the Neoarchean Eastern Dharwar Craton (compiled and reclassified by Mohan et al., 2020 after Balakrishnan and Rajamani, 1987; Bhaskar Rao et al., 1992; Dey et al., 2003, 2009, 2012, 2014; Jayananda et al., 1995, 2000; Krogstad et al., 1995; Mohan et al., 2013; Moyen et al., 2001, 2003; Prabhakar et al., 2009; Sarvothaman, 2001; Zachariah et al., 1997).

Zircon grains were extracted from orthogneisses at the Sample Separation Laboratory of the Institute of Geological Sciences, Polish Academy of Sciences in Kraków, Poland. The samples were reduced in a jaw crusher, sieved, and washed to remove fines. The magnetic fraction was removed from the concentrate using Carpco and Frantz magnetic separators. Diiodomethane with a density of 3.32 g/cm^3 was used to separate the heaviest mineral fraction. For samples containing a large amount of zircon, water panning was used instead. Zircon grains were hand-picked under a binocular microscope and cast in epoxy resin (Struers SpeciFix 20), together with standard reference materials including FC-1 (with an age of 1099 Ma, Paces and Miller, 1993) and 91,500 (80 ppm U, with an age of 1065 Ma, Wiedenbeck et al., 1995). The mounts were ground to reveal the internal structure of the grains, then polished, cleaned in an ultrasonic bath, and gold coated.

Pre-analysis imaging and U-Th-Pb isotopic analyses were performed at the Korea Basic Science Institute (KBSI) in Ochang, South Korea. Zircon grains were photographed in reflected light and imaged using a scanning electron microscope (JEOL-6610LV), with cathodoluminescence (CL) and back-scattered electron (BSE) detectors to examine the grain interiors and to choose analytical sites. Uranium-Th-Pb isotopic analyses were collected using a Sensitive High-Resolution Ion MicroProbe (SHRIMP-IIe) at KBSI. Post-analysis imaging was conducted by electron microprobe (Cameca SX-100) with a CL detector at the Faculty of Geology, University of Warsaw. The analytical procedures for SHRIMP dating followed those described by Williams (1998). A ~20 μm spot size was used for analyses, with an O_2^- primary beam intensity of 2.5–4.0 nA. Measurements were carried out in sets of five scans through nine mass stations (196 to 254 amu). Isotopic U-Th-Pb data reduction was performed by means of the SQUID 2.50 add-in for Excel 2003 (Ludwig, 2009). Common lead was corrected using the two-stage Pb isotope evolution model of Stacey and Kramers (1975). The choice of model age for common Pb has a negligible effect on age estimates for samples where the proportion of common ^{206}Pb to total ^{206}Pb is <1%. External spot-to-spot errors on measurements of the calibration standard were propagated to analyses on unknown zircon samples. The Isoplot 3.70 add-in for Excel 2003 (Ludwig, 2012) was used to generate concordia plots and to calculate weighted mean ages.

4. Samples

All samples were obtained from the archives of Geoscience Australia. The available material consisted of crushed rock powder; unfortunately, no hand specimens or thin sections were available for examination. However, the original petrographic and geochemical database of these samples is located in Sheraton et al. (1987), and the modal mineral compositions are presented in Table 1. Five samples were selected for geochemical and geochronological studies, being representative of the felsic orthogneisses of the region.

Sample RGM01 (77284538 in Sheraton et al., 1987) comes from 3 km west of Mount Bergin (Fig. 1B) in the Raggatt Mountains. It is a fine-grained, equigranular grey gneiss with granoblastic texture and is composed mostly of mesoperthite, quartz and biotite, with accessory

Table 1
Modal composition of the studied orthogneisses (after Sheraton *et al.,* 1987).

Sample	Locality	Qz	Meso	Pl	Opx	Bt	Hbl	Fe-Ti Ox	Ap	Zrn
RGM01 (77284538)	3 km west of Mount Bergin	30	61			8 (2°)	1 (2°)	a	a	a
SMT02 (76283022)	Mt Douglas	27		45	20	8		a	a	a
SMT03 (76283033)	Mt Douglas	25		60	12	3		a		a
SMT04 (77284696)	Mt Henry	27		70	3	a		a	a	a
SMT05 (77284700)	Gromov Nunataks	23		70	7			a	a	a

Mineral abbreviations: Ap – apatite; Bt – biotite; Fe-Ti Ox – Fe-Ti oxides; Hbl – hornblende; Meso – mesoperthite; Opx – orthopyroxene; Pl – plagioclase; Qz – quartz; Zrn – zircon.
2° – secondary mineral; a – accesory mineral.

hornblende, pyroxene, Fe-Ti oxides, apatite and zircon (<1 vol%). Biotite and hornblende partially or completely replace some pyroxene grains. Samples SMT02 (76283022) and SMT03 (76283033) come from Mount Douglas (Fig. 1B) in the Scott Mountains. The former is dark-grey, fine-grained, seriate and unfoliated. It is composed mostly of plagioclase, with lesser amounts of quartz, orthopyroxene and biotite. Apatite, zircon and Fe-Ti oxides are accessory phases. Sample SMT03 is dark-brown, medium-grained, seriate (0.5–4 mm) and weakly foliated. It consists mainly of plagioclase, with lesser amounts of quartz and orthopyroxene and minor biotite laths up to 4 mm long. The accessory minerals are Fe-Ti oxides and zircon. Foliation is defined by orientated biotite and flattened orthopyroxene. Sample SMT04 (77284696) was collected from Mount Henry (Fig. 1B) in the Scott Mountains and is greenish grey, medium-grained, seriate and granoblastic, without a foliation. It is composed of antiperthite and quartz, with orthopyroxene as a minor phase, and accessory Fe-Ti oxides, apatite and zircon. Sample SMT05 (77284700) was collected from Gromov Nunataks, 13 km east-southeast of Mount Henry in the Scott Mountains (Fig. 1B). It is light-brown, fine-grained, with a granoblastic texture. It is composed mostly of plagioclase, with lesser amounts of quartz and orthopyroxene, and accessory Fe-Ti oxides, apatite and zircon. A weak foliation is defined by sporadic 1 mm long grains of plagioclase in a finer-grained matrix.

5. Results

5.1. Geochemistry

Geochemical results are provided in Table 2. Gneisses analysed in this study are felsic with SiO_2 ranging from 62.7 to 70.8 wt%. Four of the samples (RGM01, SMT02, SMT03 and SMT05) plot in the granodiorite field on the Total Alkali-Silica (TAS) diagram (Fig. 2A), whereas sample SMT04 plots in the granite field. All but the latter plot in the tonalite field on the normative albite-anorthite-orthoclase triangle diagram (Fig. 2B) of Barker (1979), modified after O'Connor (1965), whereas SMT04 plots as a trondhjemite (Fig. 2B). The Alumina Saturation Index (A/CNK) ranges from 0.98 to 1.09, *i.e.,* samples are weakly peraluminous to metaluminous. All samples have low $K_2O/Na_2O < 0.5$ (Fig. 3A) and low K_2O relative to $Na_2O + CaO$. Samples RGM01 and SMT04 straddle the boundary between the high and low Al_2O_3 fields of Halla et al. (2009), whereas the remaining three samples plot in the low Al_2O_3 field (Fig. 3B). Correspondingly, the latter three samples are higher in mafic oxides ($Fe_2O_3t + MgO + MnO + TiO_2$, Fig. 3C), with all samples decreasing in mafic oxides with increasing silica. Contents of MgO vary from 0.84 to 6.88 wt% and samples SMT02, SMT03 and SMT05 (Fig. 3D) show large ranges in MgO at similar SiO_2 contents.

Following the earlier work of Sheraton and Black (1983) and Sheraton et al. (1985), Król et al. (2020) defined two chemical groups of felsic orthogneisses in the Tula Mountains of the western Napier Complex: *Group 1* with $(Y\text{-}HREE)_{sample/primitive\ mantle\ or\ S/PM} < 1$ and $(Nb\text{-}Ta)_{S/PM} = 2–7$; and *Group 2* with higher Y-HREE ($Y\text{-}HREE_{S/PM} = 3–4$) and Nb-Ta ($Nb\text{-}Ta_{S/PM} = ca.\ 10$). These groups are distinct on both the primitive mantle normalised spider diagram (Fig. 4A) and the chondrite normalised (Fig. 4B) REE diagram. Geochemical data from samples across the complex in Sheraton et al. (1987) demonstrate the widespread occurrence of these two groups. In this study, analysed samples have also been assigned to these two groups. Samples RGM01 and SMT04, with $La_N/Lu_N = 42–78$, belong to *Group 1,* whereas samples SMT02, SMT03 and SMT05 belong to *Group 2,* with $La_N/Lu_N = 10–25$. All samples have negative Nb, Ta, Ti and P anomalies (Fig. 4A). Samples RGM01, SMT04 and SMT05 display small positive Eu anomalies, whereas SMT02 and SMT03 have small negative Eu anomalies. *Group 1,* with low Y contents and hence high Sr/Y (~100) ratios, differ from *Group 2* (Fig. 5A) with high Y contents (14–18 ppm) and moderate Sr/Y ratios (~20). Similarly, *Group 1* samples have higher $(Gd/Er)_N$ ratios than *Group 2*, compared with values of ~4 rather than ~2. *Group 1* has lower transitional metal contents (including Cu, Ni and V) than *Group 2* (Table 1). There are no systematic differences between the groups in terms of high-field strength (HFS) and large ion lithophile (LIL) elements. This is also true for Rb and Th, which are highly variable in both groups.

5.2. Geochronology

Representative CL images of zircons are presented in Fig. 6. Isotopic U–Th–Pb data are presented in Tables 3–7 and plotted on Tera-Wasserburg concordia diagrams (Figs. 7–8). The reported dates in the text refer to weighted mean $^{207}Pb/^{206}Pb$ ages with the errors at 95% confidence. Discordance is defined as $^{207}Pb/^{206}Pb$ and $^{238}U/^{206}Pb$ ages that differ beyond two sigma from each other.

5.2.1. Sample SMT04, Mount Henry, Scott Mountains, Group 1 trondhjemitic orthogneiss

The zircon grains are anhedral and mostly equant (Fig. 6A), 55–180 μm in diameter, with aspect ratios varying between 1:1 and 2.5:1. Some of the grains preserve CL-dark cores with oscillatory zoning (*e.g.,* Nos. 15, 19 and 30, Fig. 6A), truncated by brighter mantles and rims with or without zoning. Such rims are variably developed and have simple concentric and sector zoning. Grains that lack CL-dark cores have sector zoning (*e.g.,* Nos. 13, 24 and 26). Most grains are free from inclusions, although radially propagated fractures are common.

A total of 45 analyses were performed on thirty grains (Table 3, Fig. 7A). Domains with concentric or sector zoning have relatively low U contents and high Th/U ratios (72–428 ppm and 0.63–3.40, respectively). Oscillatory-zoned cores have U and Th/U values of 211–1234 ppm and 0.31–1.13, respectively, whereas CL-dark zircon has high U contents (2244–3664 ppm) and low Th/U ratios (0.02–0.09). Spot $^{207}Pb/^{206}Pb$ ages scatter along the concordia but define two groups, from 2.8 to 2.6 Ga and from 2.55 to 2.40 Ga. Six data are reversely discordant. Data from concentric and sector-zoned zircon are confined to the younger group, from which the oldest nine analyses yield a weighted mean age of 2533 ± 4 Ma (MSWD = 1.2). This is interpreted as the oldest estimate for zircon growth and/or recrystallisation during metamorphism at Mt. Henry, with younger data indicating disturbance during continued metamorphism, or a subsequent event. In the older group, assuming isotopic disturbance during metamorphism, the five oldest data from oscillatory-zoned cores, typical of growth in a fractionating magma (Corfu et al., 2003; Gagnevin et al., 2010; Schaltegger

Table 2
Whole-rock major and trace element compositions of orthogneisses from the Scott and Raggatt Mountains.

Sample	RGM01 (77284538) 3 km west of Mount Bergin	SMT02 (76283022) Mt Douglas	SMT03 (76283033) Mt Douglas	SMT04 (77284696) Mt Henry	SMT05 (77284700) Gromov Nunataks
wt. %					
SiO_2	69.70	64.30	62.70	70.80	65.50
Al_2O_3	15.20	12.40	14.50	15.00	14.50
Fe_2O_{3t}	3.82	7.99	8.98	2.66	7.28
CaO	3.63	4.07	2.92	2.61	4.30
MgO	1.08	6.88	4.65	0.84	2.59
Na_2O	4.54	2.37	3.96	5.00	3.86
K_2O	1.00	0.68	1.38	2.11	0.48
MnO	0.03	0.11	0.09	0.03	0.09
TiO_2	0.41	0.46	0.64	0.37	0.78
P_2O_5	0.13	0.18	0.04	0.14	0.17
LOI	0.38	0.00	0.00	0.01	0.00
Total	99.92	99.44	99.86	99.57	99.55
ppm					
Rb	<0.10	47.50	40.50	33.30	<0.10
Ba	521.00	628.00	482.00	765.00	428.00
Sr	297.00	290.30	363.90	454.90	288.10
Ga	18.00	13.70	18.20	16.20	16.40
Hf	4.80	3.50	5.60	3.70	5.70
Nb	4.70	6.40	8.10	3.20	7.90
Ta	0.10	0.60	0.40	0.10	0.30
U	0.30	1.80	1.00	0.10	0.30
Th	1.50	11.20	32.80	0.70	0.20
Pb	0.70	3.90	4.60	1.10	0.30
V	48.00	99.00	113.00	29.00	86.00
Cu	2.10	13.20	31.10	3.90	9.10
Ni	6.60	70.80	78.80	8.60	14.60
Zr	184.20	132.20	212.50	150.80	216.60
Y	4.20	18.10	15.40	4.70	14.20
La	24.70	27.30	65.80	30.40	30.00
Ce	42.00	50.90	114.20	49.30	45.20
Pr	4.11	5.35	11.03	5.10	4.51
Nd	12.90	20.20	38.60	16.90	16.40
Sm	2.07	3.94	6.09	2.61	2.82
Eu	0.85	0.91	1.27	0.98	1.63
Gd	1.67	3.65	4.51	1.84	2.84
Tb	0.20	0.52	0.55	0.22	0.39
Dy	0.88	3.28	2.85	1.08	2.41
Ho	0.17	0.55	0.54	0.16	0.50
Er	0.38	1.87	1.68	0.37	1.62
Tm	0.06	0.25	0.24	0.05	0.24
Yb	0.34	1.63	1.67	0.34	1.73
Lu	0.06	0.26	0.27	0.04	0.30
A/CNK	1.00	1.03	1.09	0.98	0.99
A/NK	1.78	2.68	1.81	1.43	2.11
Eu/Eu*	1.39	0.73	0.74	1.36	1.76
#Mg	36	63	51	38	41

$Eu^* = \sqrt{(Sm_N * Gd_N)}$
$\#Mg = 100 * Mg/(Mg + Fe^{2+})$

and Davies, 2017), provide the most reliable estimate for the time of protolith crystallization. These data yield a weighted mean $^{207}Pb/^{206}Pb$ age of 2726 ± 6 Ma (MSWD = 2.0).

5.2.2. Sample RGM01, Mt. Bergin, Raggatt Mountains, Group 1 tonalitic orthogneiss

This sample contains anhedral to subhedral, equant to elongate zircon grains 50–400 μm in length, with aspect ratios from 1:1 to 5:1 (Fig. 6B). Several grains contain tiny (<5 μm) round inclusions. Oscillatory-zoned, elongate prismatic cores, typical of zircon crystallized from a differentiating magma, are common. Most grains have rims, with variable CL response, that truncate zoning in cores (No. 19, Fig. 6B). In CL-bright to darker rims, weak concentric zoning is dominant, and is similar to zoning in rounded grains that lack distinct cores (No. 5). Such zoning is common in zircon grown during high-temperature metamorphism (Corfu et al., 2003). A few grains have CL-dark rims (*e.g.*, No. 31) with no visible zoning, due to high contents of U.

A total of 44 analyses were carried out on 31 grains (Table 4, Fig. 7B), out of which 4 data are reversely discordant. Contents of Th and U are variable, with oscillatory-zoned domains having 156–1037 ppm U and Th/U ratios of 0.23–0.61. Metamorphic domains are characterized by either low Th/U ratios of 0.01–0.08 or high ratios of 0.82–2.20. Spot $^{207}Pb/^{206}Pb$ ages scatter along the concordia between 2.77 and 2.45 Ga. Excluding one outlier at 2773 Ma, the seven oldest data from oscillatory-zoned zircon define a magmatic age of 2711 ± 5 Ma (MSWD = 0.92). However, the outlier may indicate that all such data have been disturbed by metamorphism; if so, the mean age could be considered as a minimum age. The younger data from oscillatory-zoned cores were excluded from age calculations since these are likely to have been disturbed by metamorphism, or were analyses obtained on mixed zones (*e.g.*, No. 8, Fig. 6B).

Four data from low Th/U zircon yield a $^{207}Pb/^{206}Pb$ weighted mean age of 2529 ± 14 Ma (MSWD = 0.56). A distinct population of 7 data points from rims and grains interpreted as having grown during metamorphism, and with high Th/U, yield a $^{207}Pb/^{206}Pb$ weighted mean age

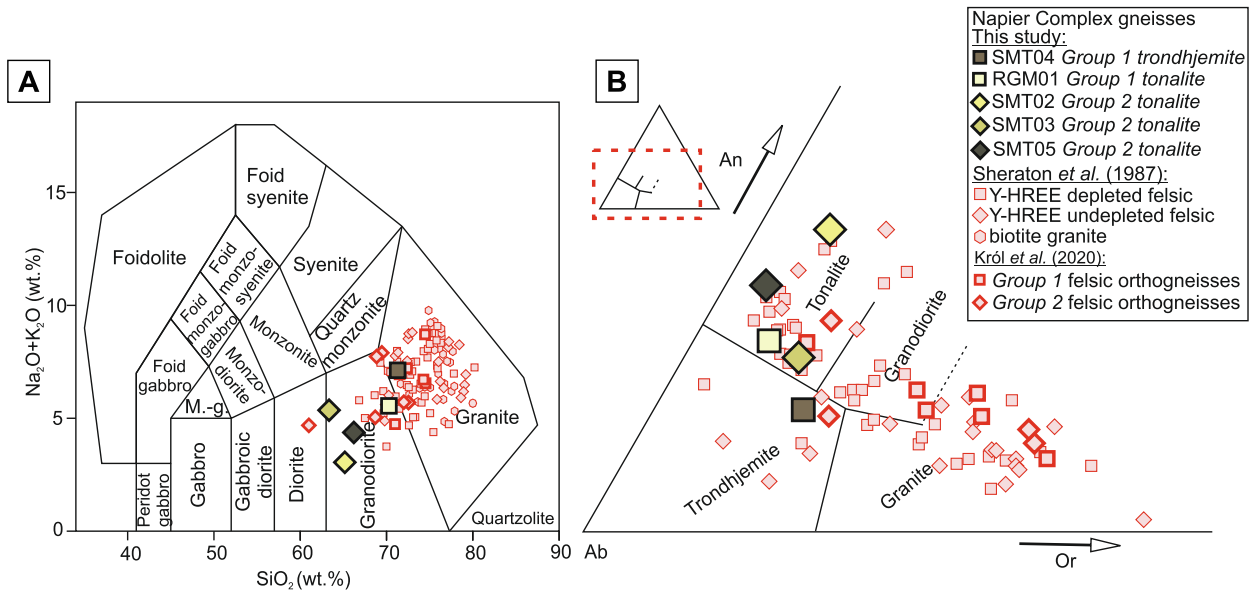

Fig. 2. Classification diagrams for orthogneisses, including published data from the eastern Tula Mountains (Król et al., 2020) and other localities in the Napier Complex (Sheraton et al., 1987). A – Total alkali *vs.* silica (TAS) diagram (Middlemost, 1994). M.–g. – Monzogabbro; Peridot. gabbro – Peridotite gabbro. B – Feldspar classification diagram (Barker, 1979, modified after O'Connor, 1965). *Group 1* and *Group 2* as defined by Król et al. (2020) represent low- and high-Y-HREE-Nb-Ta orthogneisses, respectively.

of 2478 ± 8 Ma (MSWD = 0.71). Analyses 16.2, 20.1, 24.1 and 29.1 were omitted, as analytical spots were on mixed zones or cracks. These two age populations distinguished by different Th-U contents may have grown in the presence of different accessory minerals, especially monazite (Harley and Nandakumar, 2014; Yakymchuk et al., 2018). Low Th/U zircon likely grew in the presence of monazite at *ca.* 2529 Ma, whereas high Th/U zircon likely grew at *ca.* 2478 Ma in the absence of monazite. Note, however, that monazite was not observed in the heavy minerals concentrated from this sample.

5.2.3. *Sample SMT02, Mount Douglas, Scott Mountains, Group 2 tonalitic orthogneiss*

Zircon grains are 70–180 μm in length and sub- to anhedral, equant to stubby in form, with aspect ratios ranging from 1:1 to 2:1. They have oscillatory and sector-zoned domains, either in cores (No. 8, Fig. 6C) or in the surrounding mantles (No. 1). These growth features are typical of crystallisation in a fractionating felsic magma. In many grains, cores with oscillatory zoning are well preserved (*e.g.,* No. 8), whereas the cores in other grains represent broken fragments (*e.g.,* No. 21). Magmatic growth zoning is commonly truncated by CL-dark rims, accompanied by the infilling of cracks (No. 5). Other grains have little to no visible zoning. Round inclusions of apatite, feldspar and quartz are common.

A total of 41 analyses were performed on 34 zircon grains (Table 5, Fig. 8A). Uranium and Th contents are variable, with 45–2905 ppm U and 34–2295 ppm Th, and Th/U ratios of 0.07–1.21. Spot $^{207}Pb/^{206}Pb$ ages form two distinct groups, at *ca.* 2.75 and *ca.* 2.55 Ga, with the older group represented mostly by fragmentary cores. In contrast, the younger group is dominated by zircon with distinctive oscillatory-zoned cores, along with CL-dark zircon without clear zoning. Unlike sample RGM01, zircon without zoning has mostly similar Th/U to oscillatory-zoned zircon. One outlier of *ca.* 2.9 Ga and 5 reversely discordant data are also present. Magmatic zircon yields both *ca.* 2.7 (*e.g.,* No. 21, Fig. 6C) and 2.5 Ga (*e.g.,* Nos. 1 and 8) ages. If the orthogneiss was derived from a single protolith and not a mixture of protoliths, then the younger zircon with igneous growth zoning represents the magmatic age. In this case, the older ages would be from inherited and/or xenocrystic zircon. Zircon from the younger group with the oscillatory-zoned cores and CL-dark zircon with similar Th/U ratios scatter in age along the concordia between *ca.* 2563 and 2456 Ma. The scatter can be attributed to metamorphic disturbance. Twelve out of twenty analyses on oscillatory-zoned and CL-dark zircon yield a weighted mean age of 2533 ± 5 Ma (MSWD = 1.7). However, there is an older outlier at *ca.* 2563 Ma with the same oscillatory zoning. As such, the 2533 ± 5 Ma mean age may be an underestimate for the crystallization of the protolith and should be considered as a minimum age only.

5.2.4. *Sample SMT03, Mount Douglas, Scott Mountains, Group 2 tonalitic orthogneiss*

Zircon grains are 50–180 μm in length and sub- to anhedral, with aspect ratios from 1:1 to 2:1. Many grains have cores with good internal facets and oscillatory zones (*e.g.,* Nos. 14 and 28, Fig. 6D), surrounded by CL-dark rims (*e.g.,* No. 19). Sector-zoning is also present (No. 21). There are some grains with CL-dark cores without visible zoning (*e.g.,* No. 21). Fractures cut across some grains or propagate from CL-dark cores into CL-bright domains, as a result of volume expansion due to radiation damage.

Thirty-two grains were analysed, with 44 sites selected. Spot $^{207}Pb/^{206}Pb$ ages lie along the concordia, forming distinct groups at *ca.* 2.72, 2.55 and 2.47 Ga (Table 6, Fig. 8B). Oscillatory-zoned zircon is present in the two former groups. Those with *ca.* 2.72 Ga ages have U contents of 244–1340 ppm and Th/U ratios of 0.10–8.31, whereas zircon with *ca.* 2.55 Ga ages have U < 600 ppm and Th/U ratios between 0.5 and 2.4. Zircon rims are unzoned to weakly zoned and tend to have higher U contents than cores (350–2000 ppm) and Th/U ratios of <0.4. Since older cores tend to be truncated, these are interpreted as being xenocrystic and/or inherited, whereas the *ca.* 2.55 Ga group represents crystallization of the magmatic protolith; grain 19 is an example recording ages. Nineteen data from magmatic zircon yield a $^{207}Pb/^{206}Pb$ weighted mean age of 2539 ± 5 Ma (MSWD = 1.9). Four data from rims, together with one equant unzoned grain, yield a $^{207}Pb/^{206}Pb$ weighted mean age of 2483 ± 5 Ma (MSWD = 1.12), which is interpreted as crystallization during metamorphism. The 2.52–2.50 Ga ages from zircon without visible zoning and having variable Th/U ratios, are ambiguous in origin, and were excluded from the age calculation.

5.2.5. *Sample SMT05, Gromov Nunataks, Group 2 tonalitic orthogneiss*

Zircon grains are sub- to anhedral and equant to weakly elongate,

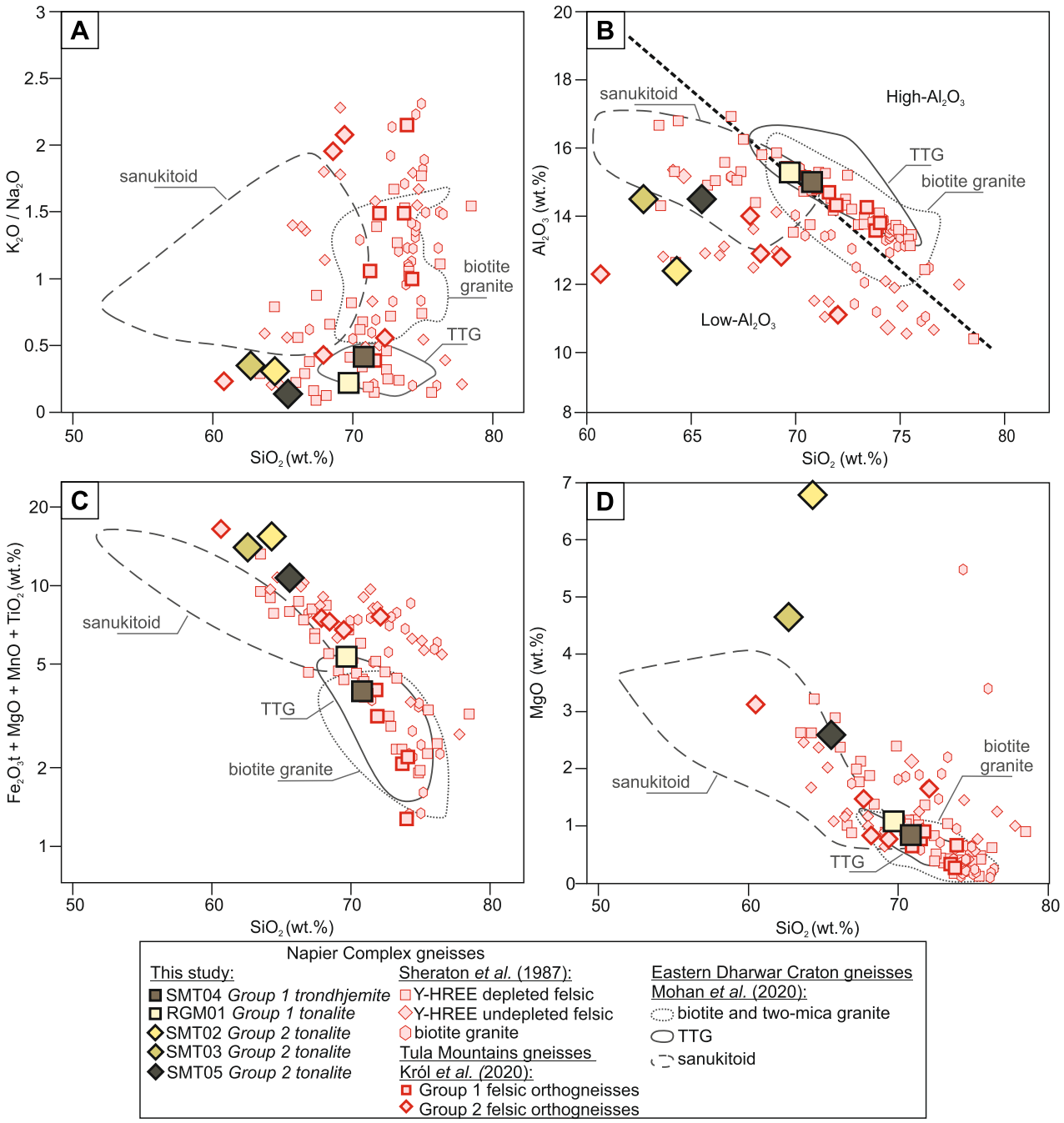

Fig. 3. Geochemical characteristics of gneisses from the southern Scott and Raggatt Mountains. Data sources include the Napier Complex (as in Fig. 2) and the Eastern Dharwar Craton (dataset compiled and reclassified by Mohan et al., 2020). A – K_2O/Na_2O *vs.* SiO_2 diagram. B – Al_2O_3 *vs.* SiO_2 diagram with high/low-Al_2O_3 fields after Halla et al. (2009). C – total ferromagnesian oxides ($Fe_2O_3t + MgO + MnO + TiO_2$) *vs.* SiO_2 diagram. D – MgO *vs.* SiO_2 diagram.

with lengths of 50–250 μm and aspect ratios of 1:1 to 1.5:1. Many grains have oscillatory zoning (*e.g.,* Nos. 4, 19 and 24; Fig. 6E), which is a common magmatic feature. Some cores are CL-dark and have no visible zoning. All grains have CL-bright rims with simple concentric zoning, which truncate zoning in the darker cores (*e.g.*, No. 18). Many grains contain inclusions of apatite and feldspar.

Forty-three sites were analysed on 30 grains (Table 6, Fig. 8C). CL-dark cores with or without oscillatory zoning have 737–2947 ppm U and 64–744 ppm Th, with Th/U ratios of 0.07–0.51. CL-bright rims have 18–173 ppm U and 7–307 ppm Th, with Th/U ratios from 0.38 to 4.83. Spot $^{207}Pb/^{206}Pb$ ages range between 2.59 and 2.35 Ga. Five data are reversely discordant. Ages from CL-dark cores with or without oscillatory zoning scatter between 2.58 and 2.50 Ga. Of these, six data yield a $^{207}Pb/^{206}Pb$ weighted mean age of 2522 ± 9 Ma (MSWD = 0.61), interpreted as a magmatic age. This may be an underestimate, considering that a similar zircon (*e.g.,* No. 24, Fig. 6E) has a slightly older $^{207}Pb/^{206}Pb$ age of *ca.* 2589 Ma. If so, the mean age can be considered as a minimum age for protolith crystallization. Six data from CL-bright rims yield an age of 2450 ± 16 Ma, interpreted as zircon growth most probably during cooling after peak metamorphic temperature was attained.

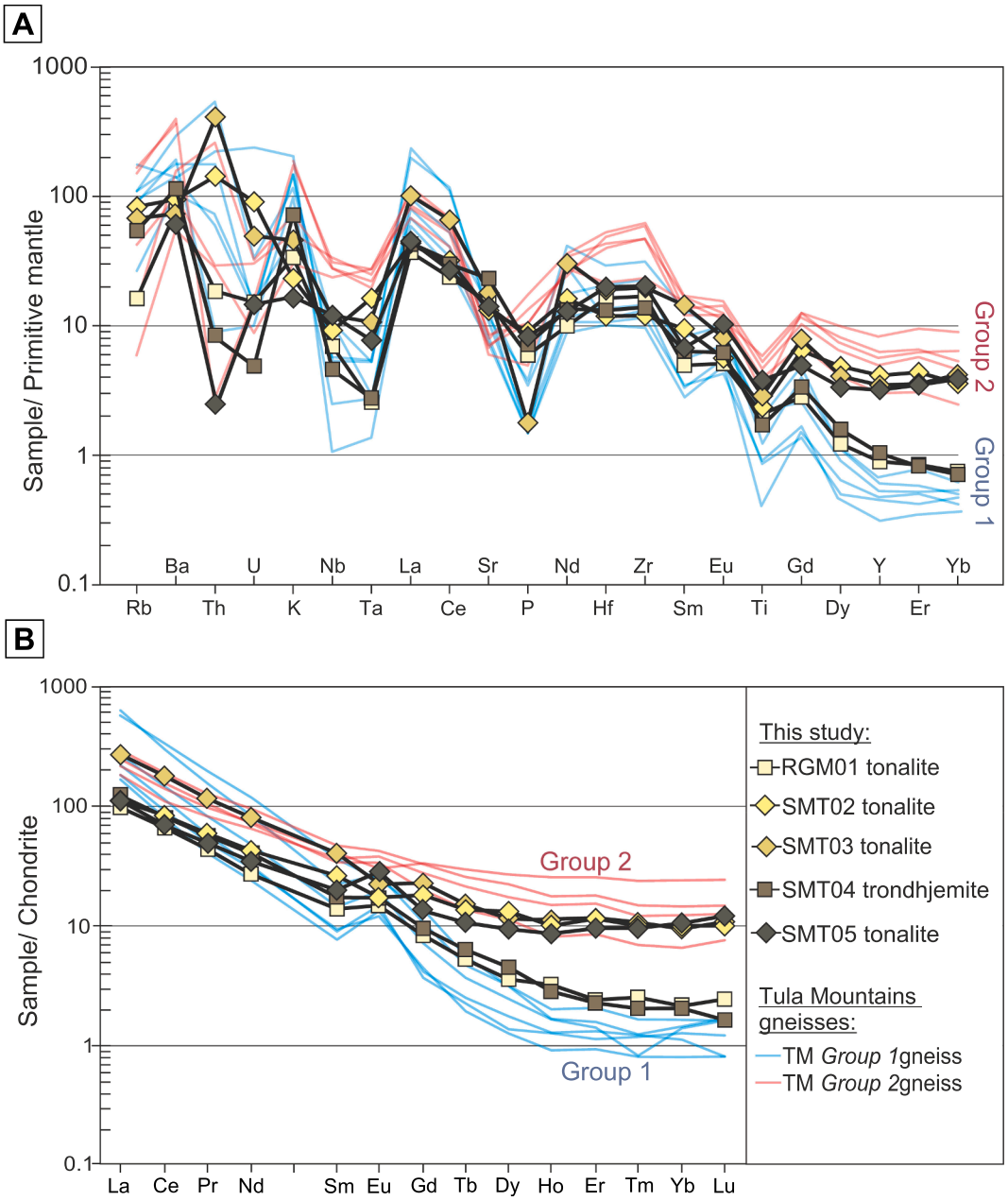

Fig. 4. A – Trace element spider diagram with elements normalised to the primitive mantle composition of McDonough and Sun (1995). B – Rare earth element (REE) diagram normalised to chondrite from McDonough and Sun (1995). Data of the Tula Mountains gneisses from Król et al., (2020).

6. Discussion

6.1. Petrogenesis

The gneisses from the Scott and Raggatt Mountains are of tonalitic-trondhjemitic composition, as defined by Barker (1979) and Jahn et al. (1981). On the classification diagram for late Archean granitoids (Fig. 9A) of Laurent et al. (2014), they plot both in the TTG field and spread into the biotite/two-mica granite field. All gneisses in the present study have low K_2O and high Na_2O/K_2O (Fig. 3A), with variations in K and Na content dependent on source composition (*e.g.,* Moyen et al., 2009; Halla, 2018). It is widely accepted that TTG magmas can be derived from the melting of hydrated basaltic crust (Barker and Arth, 1976; Rapp et al., 1991; Martin et al., 2005; Moyen and Laurent, 2018; Kendrick and Yakymchuk, 2020). Such an origin is supported by the samples plotting in the mafic source rock fields (Fig. 9B) of the discrimination diagram of Laurent et al. (2014). However, variability in Rb may be an indication that mobile elements such as K and Na were affected by fluid during metamorphism. As such, discrimination diagrams dependent on K may be suspect.

Similar to orthogneisses from the Tula Mountains (Sheraton and Black 1983; Sheraton et al., 1985; Król et al., 2020), the current samples are of two geochemical types, with either steep (*Group 1*) or flat (*Group 2)* REE patterns (Fig. 4B). The *Group 1* orthogneisses (RGM01 and SMT04) are rich in silica, aluminium (Fig. 3B) and sodium, but poor in potassium (Fig. 3A), iron and magnesium (Fig. 3C, D), which are characteristics of TTG *sensu stricto* (Barker and Arth, 1976; Moyen and Martin, 2012; Laurent et al., 2014; Moyen, 2019). These correspond to TTG of the Eastern Dharwar Craton (Mohan et al., 2020). The *Group 2* gneisses are more mafic than *Group 1* (Fig. 3), with higher contents of transitional elements (V, Cu, Ni), similar to the high-HREE group of granitoids of Halla et al. (2009). In contrast to Fe_2O_3 and V, which

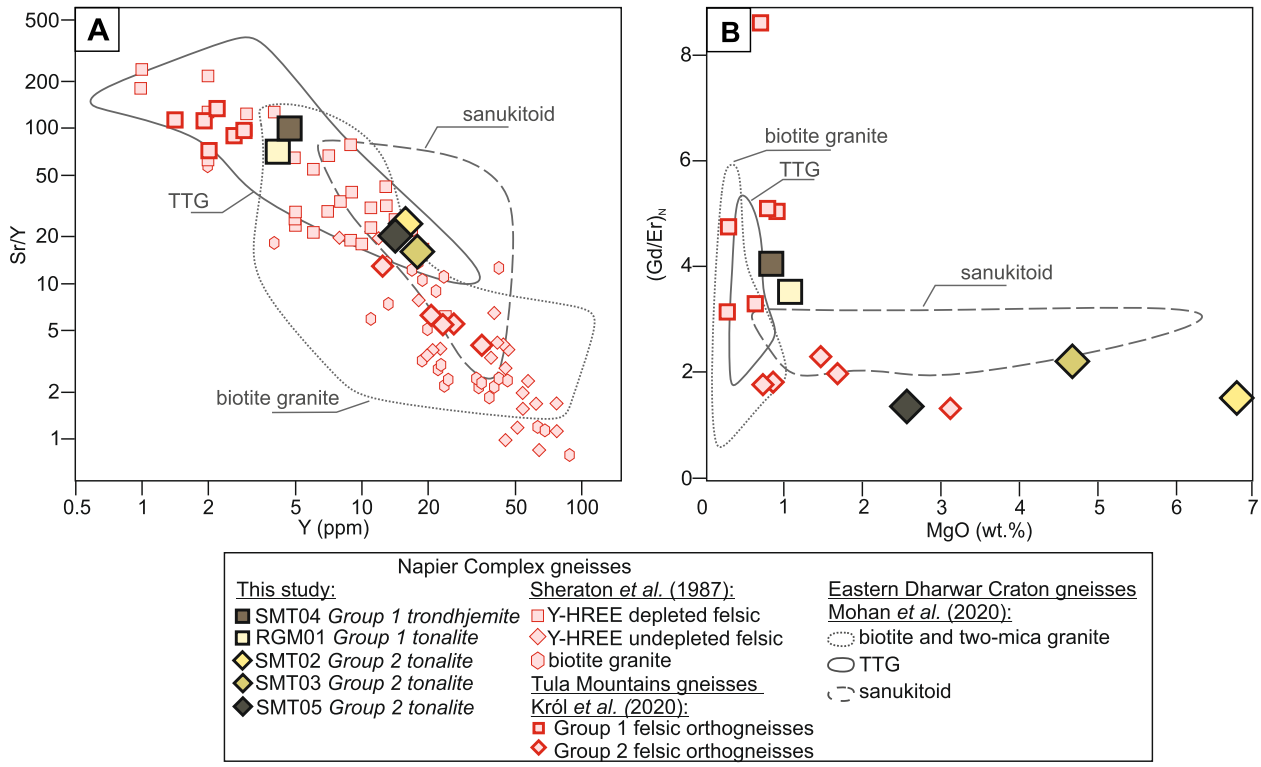

Fig. 5. Trace element binary plots. A – Sr/Y *vs.* Y. B – $(Gd/Er)_N$ *vs.* MgO. Data source as in Fig. 2.

decrease with increasing SiO_2, MgO, Cu and Ni in the *Group 2* samples are highly variable at similar SiO_2 contents. This may be due to variable amounts of peridotitic mantle or ultramafic cumulates in the source rocks. *Group 2* rocks are also distinguished by higher Nb-Ta and Y-HREE relative to *Group 1*, with flat MREE-HREE patterns (Fig. 4B) and low Sr/Y (Fig. 5A); and $(Gd/Yb)_N$ (Fig. 5B). This is similar to the low-Al_2O_3 granitoids defined by Halla et al. (2009).

Yttrium, HREE, Nb-Ta, and Sr contents are commonly used to estimate the depth at which TTG melts originate from a basaltic source. The stability of minerals sequestering these elements, *i.e.,* plagioclase, garnet, and rutile, is mostly pressure dependant (Defant and Drummond, 1990; Moyen and Stevens, 2006; Kendrick and Yakymchuk, 2020). In mafic rocks, garnet is stable at pressures above 1.0–1.2 GPa (Moyen and Stevens, 2006; White et al., 2017, Kendrick and Yakymchuk, 2020) and rutile at 1.6–1.9 GPa (Moyen and Stevens, 2006), whereas the stability of plagioclase is commonly constrained to <1.5 GPa (Kendrick and Yakymchuk, 2020). The steep REE pattern of *Group 1* samples (Fig. 4B), with low Y-HREE, high Sr/Y, and high $(Gd/Er)_N$, could be attributed to the presence of considerable amounts of garnet in the restite. Likewise, low Nb, Ta and Ti can be attributed to the presence of rutile. The lack of plagioclase in the restite can account for high Al_2O_3 together with high Sr/Y and the small positive Eu anomaly. *Group 1* rocks have Nb and Ta contents of 3.2–4.7 ppm and 0.1 ppm, respectively, typical of magma generation at medium- (*ca.* 1.5 GPa) to high-pressure (>2.0 GPa) melting (Moyen, 2011). Therefore, *Group 1* rocks may have been generated under pressures of at least 1.5 GPa with garnet, some rutile, and no plagioclase in the restite. The geochemical characteristics of *Group* 2 can be accounted for by the presence of plagioclase in the restite and the absence of garnet and rutile, corresponding to pressures of <1.2 GPa.

This simple pressure-dependent relationship has recently been challenged. Smithies et al. (2019) suggested that the high-pressure TTG signature can be produced by amphibole fractionation of melts derived from metasomatically-enriched lithospheric mantle. Pourteau et al. (2020) indicated that fluid-fluxed melting at <30 km of mafic rocks, during which plagioclase is consumed and amphibole remains in the residue, can produce melts with high Sr and low REE. The stability of garnet has also been shown to depend significantly on the bulk source composition (Johnson et al., 2017) and temperature (Kendrick and Yakymchuk, 2020). Johnson et al. (2017) showed that low #Mg in basaltic source rocks allows garnet and rutile to stabilise at pressures down to 0.7–0.8 GPa, whereas Kendrick and Yakymchuk (2020) showed that above 900 °C, the modal proportion of garnet decreases with increasing P-T, hence increasing the availability of garnet-compatible elements (Y-HREE) in the melt. However, such low #Mg mafic rocks are not abundant in the Napier Complex (Sheraton et al. 1987). Moreover, the use of Nb and Ta alone to determine depth of melting can lead to misinterpretations, as these elements are strongly dependent on bulk composition (*e.g.,* Kendrick and Yakymchuk, 2020). Nevertheless, the consistency of various depth-dependent indicators, *i.e.,* Y-HREE and Nb-Ta contents, Sr/Y, $(Gd/Er)_N$ and La_N/Yb_N corroborates the interpretation that *Group 1* rocks were likely generated under pressures of at least 1.5 GPa.

6.2. *Timing of geological events in the Neoarchean of the Napier Complex*

6.2.1. *Significance of ca. 2.7 Ga ages*

A summary of age estimates for igneous and metamorphic events in the Napier Complex, as obtained from orthogneisses from this and other studies, is presented in Fig. 10. Eoarchean ages have only been identified in the Tula Mountains in Enderby Land (Harley et al., 2019; Król et al., 2020), and Aker Peaks in Kemp Land (Kusiak et al., 2021). Magmatism between 3.3 and 2.8 Ga is more widespread, with localities extending from Proclamation Island (Kelly and Harley, 2005) to the Tula Mountains (*e.g.,* Harley and Black, 1997; Król et al., 2020). Protolith ages that postdate *ca.* 2.8 Ga metamorphism have been recognised only in this study in the southwest of the complex, at the Fyfe Hills and Casey Bay (*ca.* 2.7 Ga, Horie et al., 2012) and on Tonagh Island (*ca.* 2.6 Ga, Carson et al., 2002a; Crowe et al., 2002).

The present study provides new ages for protolith crystallization at

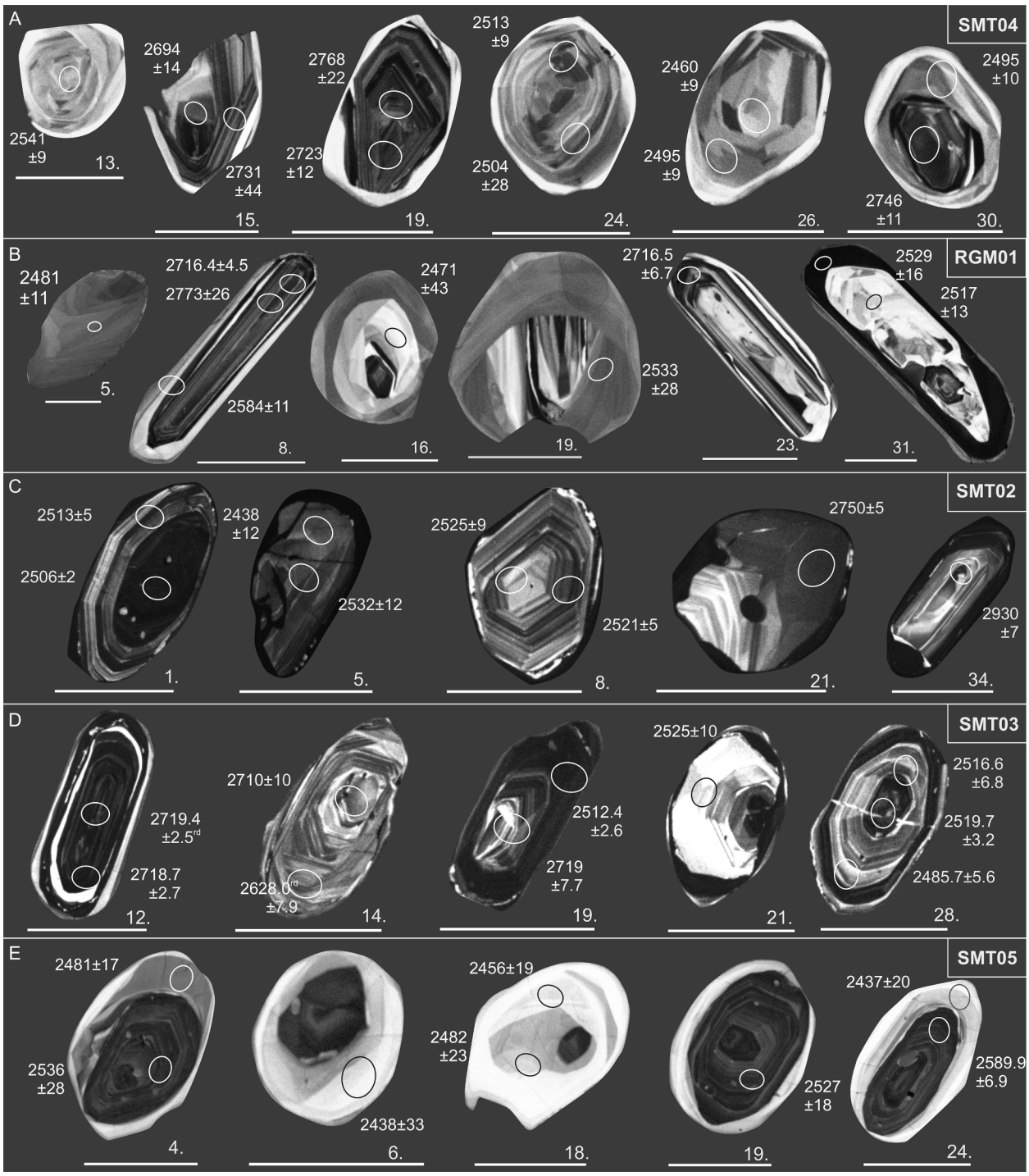

Fig. 6. Representative cathodoluminescence images of zircon in samples from the Scott and Raggatt Mountains. Solid ellipses represent sites of U-Pb analyses, labelled with $^{207}Pb/^{206}Pb$ ages in Ma. The grain numbers in figure refer to the grain numbers in Tables 3–7. Errors are 1 sigma. A – SMT04. B – RGM02. C – SMT02. D – SMT03. E – SMT05. Scale bars are 100 μm.

Table 3
U–Th–Pb data for sample SMT04 from Mount Henry.

Analysis					Ratios[a]							Ages[a]				
(Grain.spot)	U (ppm)	Th (ppm)	Th/U	$^{206}Pb_c$(%)[b]	$^{238}U/^{206}Pb$	±σ (%)	$^{207}Pb/^{206}Pb$	±σ (%)	$^{207}Pb/^{235}U$	±σ (%)	ρ[c]	$^{206}Pb/^{238}U$	±σ	$^{207}Pb/^{206}Pb$	±σ	Conc. (%)[d]
Prismatic cores with oscilatory zoning																
19.1	754	422	0.56	—	1.830	2.4	0.1930	1.3	14.54	2.7	0.88	2810	58	2768	22	102
30.1	476	300	0.63	0.02	1.841	2.3	0.19044	0.64	14.26	2.4	0.96	2799	56	2746	11	102
15.2	383	178	0.47	0.02	1.790	2.4	0.1887	2.6	14.54	3.6	0.68	2867	59	2731	44	106
22.1	725	1131	1.56	0.01	1.840	2.3	0.18784	0.19	14.08	2.3	1.0	2801	64	2723.3	3.1	103
19.2	363	158	0.44	0.02	1.857	2.3	0.18780	0.70	13.94	2.4	0.96	2777	55	2723	12	102
8.1	*1234*	*907*	*0.73*	*0.01*	*1.852*	*2.2*	*0.18275*	*0.42*	*13.61*	*2.2*	*0.98*	*2785*	*54*	*2678.0*	*7.0*	*105*
12.1	*159*	*115*	*0.73*	*0.09*	*2.013*	*2.4*	*0.18111*	*0.50*	*12.40*	*2.5*	*0.98*	*2599*	*56*	*2663.1*	*8.3*	*97*
12.2	*215*	*67*	*0.31*	*0.05*	*1.943*	*2.7*	*0.1809*	*1.8*	*12.84*	*3.2*	*0.82*	*2678*	*60*	*2661*	*30*	*101*
21.1	*613*	*515*	*0.84*	—	*2.074*	*2.5*	*0.17281*	*0.23*	*11.49*	*2.5*	*1.0*	*2532*	*57*	*2585.0*	*3.9*	*98*
10.1	*523*	*294*	*0.56*	*0.08*	*2.087*	*2.4*	*0.1640*	*1.0*	*10.83*	*2.6*	*0.92*	*2526*	*54*	*2497*	*17*	*101*
25.3	*211*	*238*	*1.13*	*0.01*	*2.060*	*2.6*	*0.1614*	*1.0*	*10.80*	*2.8*	*0.94*	*2558*	*63*	*2470*	*16*	*104*
Sector-zoned domain																
16.1	81	3	0.03	0.05	2.058	2.3	0.16704	0.79	11.19	2.5	0.95	2554	49	2528	13	101
Domains with irregular concentric or chaotic zoning																
29.1	145	145	1.00	—	2.069	2.7	0.16852	0.52	11.23	2.7	0.98	2549	64	2543.0	8.7	100
13.1	144	428	2.97	—	2.016	2.3	0.16834	0.55	11.51	2.3	0.97	2591	75	2541.2	9.2	103
17.1	146	310	2.12	0.03	2.054	2.3	0.16810	0.57	11.28	2.3	0.97	2551	64	2539	10	101
24.1	132	393	2.97	—	2.042	2.3	0.16560	0.55	11.18	2.4	0.97	2574	75	2513.7	9.3	103
24.2	157	354	2.25	0.39	2.077	2.3	0.1647	1.6	10.93	2.8	0.81	2536	65	2504	28	101
30.2	*141*	*194*	*1.37*	*0.05*	*2.193*	*2.3*	*0.16377*	*0.59*	*10.30*	*2.3*	*0.97*	*2422*	*55*	*2495*	*10*	*96*
7.2	*242*	*175*	*0.72*	*0.03*	*2.091*	*2.2*	*0.16376*	*0.46*	*10.80*	*2.3*	*0.98*	*2519*	*51*	*2494.8*	*7.7*	*101*
26.2	*125*	*380*	*3.03*	*0.01*	*2.140*	*2.3*	*0.16375*	*0.61*	*10.55*	*2.4*	*0.97*	*2499*	*73*	*2495*	*10*	*99*
25.2	*329*	*276*	*0.84*	—	*2.031*	*2.4*	*0.16315*	*0.79*	*11.07*	*2.5*	*0.95*	*2588*	*57*	*2489*	*13*	*104*
6.1	*95*	*323*	*3.40*	—	*2.014*	*2.7*	*0.16143*	*0.77*	*11.05*	*2.8*	*0.96*	*2594*	*99*	*2471*	*13*	*106*
14.2	*165*	*260*	*1.58*	*0.08*	*2.088*	*2.3*	*0.16118*	*0.56*	*10.64*	*2.3*	*0.97*	*2540*	*58*	*2468.0*	*9.4*	*103*
27.1	*72*	*155*	*2.16*	*0.02*	*2.182*	*2.3*	*0.16057*	*0.81*	*10.15*	*2.5*	*0.94*	*2447*	*63*	*2462*	*14*	*99*
9.1	*145*	*266*	*1.83*	*0.06*	*2.101*	*2.3*	*0.16051*	*0.59*	*10.54*	*2.3*	*0.97*	*2521*	*60*	*2461*	*10*	*102*
26.1	*133*	*387*	*2.91*	*0.02*	*2.139*	*2.6*	*0.16037*	*0.62*	*10.34*	*2.6*	*0.97*	*2526*	*79*	*2460*	*10*	*101*
21.2	*159*	*300*	*1.89*	*0.00*	*2.140*	*2.3*	*0.16022*	*0.50*	*10.32*	*2.4*	*0.98*	*2470*	*62*	*2458.0*	*8.5*	*101*
11.1	*125*	*288*	*2.31*	*0.04*	*2.076*	*2.5*	*0.15960*	*0.64*	*10.60*	*2.6*	*0.97*	*2541*	*73*	*2451*	*11*	*104*
28.1	*75*	*134*	*1.80*	*0.07*	*2.122*	*2.3*	*0.15909*	*0.81*	*10.34*	*2.5*	*0.94*	*2502*	*61*	*2446*	*14*	*102*
16.2	*128*	*336*	*2.61*	*0.02*	*2.196*	*2.3*	*0.15852*	*0.59*	*9.951*	*2.4*	*0.97*	*2440*	*67*	*2440*	*10*	*99*
23.1	*68*	*160*	*2.34*	*0.06*	*2.113*	*2.3*	*0.15769*	*0.88*	*10.29*	*2.5*	*0.94*	*2510*	*67*	*2431*	*15*	*103*
2.1	*115*	*103*	*0.89*	*0.13*	*2.133*	*2.3*	*0.15684*	*0.69*	*10.14*	*2.4*	*0.96*	*2481*	*53*	*2422*	*12*	*103*
1.3	*89*	*256*	*2.88*	*0.35*	*2.082*	*2.3*	*0.1548*	*1.0*	*10.25*	*2.6*	*0.91*	*2539*	*75*	*2400*	*18*	*106*
Domains without visible zoning																
15.1	*476*	*291*	*0.61*	*0.02*	*1.902*	*2.4*	*0.18454*	*0.84*	*13.38*	*2.6*	*0.94*	*2730*	*57*	*2694*	*14*	*101*
7.1	*544*	*265*	*0.49*	*0.02*	*1.956*	*2.6*	*0.1760*	*2.1*	*12.41*	*3.3*	*0.78*	*2662*	*60*	*2616*	*34*	*102*
4.1	2425	37	0.02	—	1.963	2.2	0.16760	0.50	11.77	2.3	0.98	2654	48	2533.8	8.4	106
25.1	3485	297	0.09	0.00	1.913	2.3	0.16706	0.27	12.04	2.3	0.99	2712	52	2528.4	4.5	109
5.1	*3664*	*247*	*0.07*	*0.00*	*1.870*	*2.2*	*0.16457*	*0.11*	*12.13*	*2.2*	*1.0*	*2761*	*50*	*2503.1*	*1.8*	*113*
1.2	*2842*	*148*	*0.05*	*0.00*	*1.937*	*2.2*	*0.16383*	*0.12*	*11.66*	*2.2*	*1.0*	*2684*	*49*	*2495.6*	*2.0*	*109*
Analyses on mixtures of zones or cracked grain																
20.1	*196*	*71*	*0.36*	*0.05*	*1.923*	*3.2*	*0.1800*	*3.0*	*12.91*	*4.4*	*0.73*	*2702*	*74*	*2653*	*50*	*102*
14.1	*2663*	*76*	*0.03*	*0.00*	*1.912*	*2.2*	*0.16651*	*0.60*	*12.01*	*2.3*	*0.96*	*2712*	*49*	*2523*	*10*	*109*
3.1	*3196*	*52*	*0.02*	*0.00*	*1.885*	*2.2*	*0.16571*	*0.27*	*12.12*	*2.2*	*0.99*	*2743*	*50*	*2514.8*	*4.6*	*111*
1.1	*504*	*331*	*0.66*	*0.01*	*2.068*	*2.2*	*0.16551*	*0.91*	*11.03*	*2.4*	*0.93*	*2538*	*50*	*2513*	*15*	*101*
18.1	*1975*	*75*	*0.04*	*0.01*	*1.988*	*2.3*	*0.16504*	*0.14*	*11.45*	*2.3*	*1.0*	*2627*	*49*	*2507.9*	*2.3*	*106*
17.2	*70*	*185*	*2.63*	—	*2.045*	*2.7*	*0.16248*	*0.90*	*10.95*	*2.8*	*0.95*	*2578*	*82*	*2482*	*15*	*104*

[a]Values corrected for common Pb.
[b]Percentage ^{206}Pb which is non-radiogenic.
[c]Error correlation between $^{238}U/^{206}Pb$ and $^{207}Pb/^{235}U$.
[d]Conc. (%): concordance = 100 (1 - $^{206}Pb/^{238}U$ /($e^{0.000155125a}$ −1)), where a is the $^{207}Pb/^{206}Pb$ age. Analyses in italics not used for concordia age.

Table 4
U–Th–Pb data for sample RGM01 from 3 km west of Mount Bergin.

Analysis					Ratios[a]							Ages[a]				
(Grain.spot)	U (ppm)	Th (ppm)	Th/U	$^{206}Pb_c$(%)[b]	$^{238}U/^{206}Pb$	±σ (%)	$^{207}Pb/^{206}Pb$	±σ (%)	$^{207}Pb/^{235}U$	±σ (%)	ρ[c]	$^{206}Pb/^{238}U$	±σ	$^{207}Pb/^{206}Pb$	±σ	Conc. (%)[d]
Oscillatory-zoned domains																
8.1	*553*	*133*	*0.24*	*0.03*	*1.777*	*4.9*	*0.194*	*1.6*	*15.02*	*5.2*	*0.95*	*2867*	*117*	*2773*	*26*	*105*
11.2	156	70	0.45	0.01	1.944	1.8	0.1874	0.87	13.29	2.0	0.90	2678	41	2719	14	98
23.2	642	237	0.37	0.06	1.866	1.7	0.1871	0.41	13.82	1.7	0.97	2765	39	2716.5	6.7	102
8.3	514	116	0.23	0.01	1.882	2.1	0.1870	0.27	13.70	2.1	0.99	2746	47	2716.4	4.5	101
3.1	514	115	0.22	0.08	1.765	2.2	0.1864	0.33	14.56	2.3	0.99	2897	54	2710.6	5.4	108
14.2	402	150	0.37	0.01	1.864	1.7	0.186	1.0	13.75	2.0	0.86	2771	40	2707	17	103
21.1	994	407	0.41	0.03	1.879	2.4	0.1858	0.22	13.63	2.5	1.00	2753	57	2705.3	3.7	102
28.2	*276*	*134*	*0.49*	*0.01*	*1.887*	*1.8*	*0.1847*	*0.36*	*13.49*	*1.8*	*0.98*	*2750*	*43*	*2695.7*	*5.9*	*102*
28.1	*228*	*138*	*0.61*	—	*1.868*	*1.7*	*0.1809*	*0.86*	*13.35*	*1.9*	*0.90*	*2765*	*41*	*2661*	*14*	*105*
22.2	*358*	*160*	*0.45*	*0.03*	*1.997*	*1.8*	*0.1776*	*0.37*	*12.26*	*1.8*	*0.98*	*2620*	*40*	*2630.4*	*6.2*	*99*
11.1	*199*	*94*	*0.47*	—	*1.990*	*4.0*	*0.177*	*2.1*	*12.25*	*4.5*	*0.88*	*2627*	*91*	*2623*	*36*	*100*
25.2	*1037*	*292*	*0.28*	*0.04*	*1.914*	*1.7*	*0.1761*	*0.47*	*12.69*	*1.7*	*0.96*	*2715*	*38*	*2616.3*	*7.8*	*104*
Irregularly zoned domains																
19.1	266	252	0.95	—	2.096	5.0	0.168	1.7	11.02	5.2	0.95	2518	115	2533	28	99
9.1	329	228	0.69	—	2.261	3.7	0.166	2.7	10.14	4.5	0.81	2359	79	2521	45	92
27.2	263	302	1.15	0.01	2.124	1.7	0.1631	0.46	10.59	1.8	0.97	2488	41	2487.7	7.7	100
5.1	200	348	1.75	—	2.074	2.3	0.1624	0.66	10.80	2.4	0.96	2546	61	2481	11	103
30.2	257	386	1.50	0.03	2.147	1.7	0.1623	0.51	10.42	1.8	0.96	2464	43	2479.3	8.5	99
4.1	163	240	1.47	—	2.017	2.3	0.1620	0.68	11.07	2.4	0.96	2607	60	2476	11	106
16.1	51	113	2.20	0.01	1.908	22.7	0.161	2.6	11.67	23	0.99	2807	661	2471	43	112
27.1	146	258	1.77	0.04	2.039	1.8	0.1607	0.57	10.86	1.9	0.95	2576	48	2463	10	105
17.1	110	215	1.95	0.04	1.973	2.5	0.160	4.4	11.17	5.1	0.49	2666	71	2453	75	109
18.1	*297*	*244*	*0.82*	*0.03*	*2.253*	*4.9*	*0.1588*	*0.60*	*9.722*	*4.9*	*0.99*	*2346*	*110*	*2443*	*10*	*96*
Low Th/U recrystallised domains																
15.1	3491	271	0.08	0.06	2.105	4.2	0.169	1.1	11.04	4.4	0.97	2505	89	2543	19	98
6.1	2099	132	0.06	0.00	1.997	2.2	0.1678	0.76	11.59	2.3	0.95	2618	48	2536	13	104
31.2	2682	20	0.01	0.00	2.039	1.9	0.1671	0.97	11.30	2.2	0.89	2573	41	2529	16	102
31.1	88	0.2	0.002	0.05	2.083	1.9	0.1660	0.75	10.99	2.0	0.93	2528	39	2517	13	100
2.1	*4483*	*170*	*0.04*	*0.00*	*1.947*	*2.3*	*0.1617*	*0.57*	*11.45*	*2.3*	*0.97*	*2672*	*50*	*2473*	*10*	*110*
Patchy domains																
12.1	68	0.3	0.005	—	2.059	2.6	0.185	1.3	12.38	2.9	0.90	2544	54	2698	21	93
25.1	*3197*	*486*	*0.15*	*0.01*	*1.791*	*1.7*	*0.1743*	*0.40*	*13.42*	*1.7*	*0.97*	*2859*	*40*	*2599.4*	*6.7*	*112*
Core without visible zoning																
20.1	*105*	*162*	*1.54*	—	*1.908*	*5.4*	*0.165*	*1.9*	*11.91*	*5.7*	*0.94*	*2746*	*143*	*2506*	*32*	*110*
Analyses on mixtures of zones; cracked zircon																
13.1	1359	101	0.07	0.04	1.617	10.0	0.1849	1.00	15.76	10.1	1.00	3105	248	2697	16	119
14.1	*352*	*126*	*0.36*	*0.04*	*1.928*	*7.4*	*0.1840*	*0.45*	*13.16*	*7.4*	*1.00*	*2692*	*170*	*2689.2*	*7.5*	*100*
14.3	*159*	*46*	*0.29*	*0.06*	*1.988*	*2.0*	*0.1805*	*0.55*	*12.52*	*2.0*	*0.96*	*2627*	*44*	*2657.5*	*9.2*	*99*
25.3	*2817*	*256*	*0.09*	*0.02*	*1.846*	*1.7*	*0.1776*	*0.45*	*13.26*	*1.7*	*0.97*	*2792*	*38*	*2630.8*	*7.4*	*107*
26.1	*782*	*55*	*0.07*	*0.11*	*2.016*	*2.2*	*0.1758*	*0.29*	*12.02*	*2.2*	*0.99*	*2597*	*47*	*2613.7*	*4.8*	*99*
1.1	*658*	*204*	*0.31*	*0.01*	*1.970*	*2.8*	*0.1755*	*0.77*	*12.28*	*2.9*	*0.96*	*2646*	*62*	*2611*	*13*	*102*
24.2	*352*	*121*	*0.34*	*0.05*	*1.962*	*2.1*	*0.175*	*1.3*	*12.27*	*2.5*	*0.85*	*2662*	*48*	*2602*	*22*	*102*
8.2	*788*	*114*	*0.14*	*0.12*	*2.085*	*1.7*	*0.1728*	*0.64*	*11.42*	*1.8*	*0.93*	*2518*	*36*	*2585*	*11*	*97*
10.1	*850*	*386*	*0.45*	*0.02*	*2.060*	*2.2*	*0.1704*	*0.45*	*11.41*	*2.3*	*0.98*	*2554*	*49*	*2561.9*	*7.5*	*99*
29.1	*424*	*198*	*0.47*	*0.10*	*2.092*	*1.7*	*0.1670*	*0.57*	*11.01*	*1.8*	*0.95*	*2520*	*37*	*2528*	*10*	*100*
24.1	*319*	*123*	*0.39*	*0.22*	*2.133*	*1.7*	*0.1660*	*0.45*	*10.73*	*1.8*	*0.97*	*2479*	*37*	*2517.3*	*7.6*	*98*
7.1	72	68	0.95	—	2.024	3.7	0.161	1.7	10.94	4.1	0.91	2605	88	2461	28	106
30.1	*440*	*108*	*0.24*	—	*2.141*	*1.7*	*0.1603*	*0.34*	*10.33*	*1.7*	*0.98*	*2473*	*36*	*2459.0*	*5.7*	*101*
16.2	*293*	*286*	*0.97*	*0.02*	*2.062*	*1.7*	*0.1636*	*0.40*	*10.94*	*1.8*	*0.97*	*2552*	*41*	*2493.2*	*6.8*	*103*

[a]Values corrected for common Pb.
[b]Percentage ^{206}Pb which is non-radiogenic.
[c]Error correlation between $^{238}U/^{206}Pb$ and $^{207}Pb/^{235}U$.
[d]Conc. (%): concordance = 100 (1 - $^{206}Pb/^{238}U$ /($e^{0.000155125a}$ −1)), where a is the $^{207}Pb/^{206}Pb$ age. Analyses in italics not used for concordia age.

Table 5
U–Th–Pb data for sample SMT02 from Mount Douglas.

Analysis					Ratios[a]							Ages[a]				
(Grain.spot)	U (ppm)	Th (ppm)	Th/U	$^{206}Pb_c$(%)[b]	$^{238}U/^{206}Pb$	±σ (%)	$^{207}Pb/^{206}Pb$	±σ (%)	$^{207}Pb/^{235}U$	±σ (%)	ρ[c]	$^{206}Pb/^{238}U$	±σ	$^{207}Pb/^{206}Pb$	±σ	Conc. (%)[d]
Oscillatory or sector-zoned cores																
34.1	*162*	*99*	*0.61*	—	*1.732*	*2.3*	*0.21324*	*0.46*	*16.97*	*2.32*	*0.98*	*2938*	*57*	*2930.3*	*7.5*	*100*
21.1	*348*	*211*	*0.61*	*0.02*	*1.861*	*2.2*	*0.19092*	*0.32*	*14.15*	*2.25*	*0.99*	*2773*	*54*	*2750.1*	*5.2*	*101*
11.1	*1893*	*2295*	*1.21*	*0.00*	*1.768*	*2.2*	*0.18935*	*0.73*	*14.76*	*2.32*	*0.95*	*2893*	*59*	*2737*	*12*	*107*
28.1	*144*	*81*	*0.56*	*0.04*	*1.872*	*2.3*	*0.18851*	*0.51*	*13.89*	*2.33*	*0.98*	*2761*	*54*	*2729.2*	*8.3*	*101*
19.1	*45*	*34*	*0.76*	*0.21*	*1.856*	*2.9*	*0.1863*	*1.0*	*13.84*	*3.11*	*0.94*	*2781*	*72*	*2710*	*17*	*103*
12.1	*949*	*877*	*0.92*	*0.00*	*1.858*	*2.3*	*0.18556*	*0.37*	*13.77*	*2.31*	*0.99*	*2779*	*57*	*2703.2*	*6.2*	*103*
2.2	*672*	*370*	*0.55*	*0.00*	*1.857*	*2.2*	*0.18554*	*0.48*	*13.77*	*2.27*	*0.98*	*2780*	*53*	*2703.0*	*7.9*	*103*
2.1	*386*	*148*	*0.38*	*0.00*	*1.885*	*2.2*	*0.1854*	*1.0*	*13.56*	*2.43*	*0.92*	*2742*	*52*	*2702*	*16*	*102*
20.1	*205*	*178*	*0.86*	—	*1.907*	*2.3*	*0.18504*	*0.43*	*13.38*	*2.29*	*0.98*	*2724*	*55*	*2698.5*	*7.1*	*101*
18.1	*600*	*340*	*0.57*	*0.00*	*1.890*	*2.2*	*0.18197*	*0.24*	*13.28*	*2.23*	*0.99*	*2739*	*53*	*2670.9*	*4.0*	*103*
32.2	*168*	*82*	*0.49*	*0.09*	*1.908*	*2.3*	*0.17413*	*0.62*	*12.59*	*2.36*	*0.97*	*2723*	*53*	*2598*	*10*	*106*
10.1	*355*	*192*	*0.54*	*0.01*	*2.026*	*2.2*	*0.17056*	*0.36*	*11.61*	*2.26*	*0.99*	*2591*	*50*	*2563.1*	*6.0*	*101*
26.1	*81*	*67*	*0.82*	*0.04*	*2.032*	*2.3*	*0.17033*	*0.77*	*11.56*	*2.45*	*0.95*	*2580*	*54*	*2561*	*13*	*101*
23.1	489	326	0.67	0.01	1.980	2.5	0.16886	0.34	11.76	2.49	0.99	2636	57	2546.4	5.7	104
14.1	662	432	0.65	0.00	2.031	2.2	0.16766	0.24	11.38	2.23	0.99	2583	51	2534.5	4.1	102
27.1	270	219	0.81	—	2.060	2.2	0.16678	0.42	11.16	2.28	0.98	2552	52	2525.6	7.0	101
8.1	154	111	0.72	0.02	2.115	2.3	0.16674	0.56	10.87	2.34	0.97	2504	51	2525.2	9.4	99
31.2	357	163	0.46	0.02	2.063	2.3	0.16656	0.33	11.13	2.36	0.99	2556	52	2523.4	5.5	101
8.2	413	379	0.92	0.02	2.073	2.2	0.16642	0.32	11.07	2.25	0.99	2555	52	2522.0	5.3	101
15.1	133	70	0.52	0.08	2.018	2.3	0.1660	1.4	11.34	2.67	0.86	2597	52	2517	23	104
33.1	89	57	0.64	0.08	2.115	2.3	0.16580	0.81	10.81	2.47	0.94	2494	52	2516	14	99
1.2	*469*	*239*	*0.51*	—	*2.072*	*2.2*	*0.16557*	*0.30*	*11.02*	*2.24*	*0.99*	*2543*	*49*	*2513.4*	*5.1*	*101*
14.2	*433*	*197*	*0.45*	*0.03*	*2.079*	*2.6*	*0.16544*	*0.32*	*10.97*	*2.57*	*0.99*	*2533*	*56*	*2512.0*	*5.5*	*101*
7.1	*1169*	*841*	*0.72*	*0.00*	*2.019*	*2.2*	*0.16210*	*0.18*	*11.07*	*2.22*	*1.0*	*2596*	*51*	*2477.6*	*3.1*	*106*
25.1	*271*	*201*	*0.74*	*0.04*	*2.105*	*2.2*	*0.15999*	*0.40*	*10.48*	*2.27*	*0.98*	*2503*	*51*	*2455.6*	*6.8*	*102*
Domains without visible zoning																
9.1	*349*	*145*	*0.42*	*0.01*	*1.971*	*2.2*	*0.18934*	*0.97*	*13.25*	*2.43*	*0.92*	*2647*	*51*	*2736*	*16*	*96*
17.1	*901*	*448*	*0.50*	*0.01*	*1.896*	*2.4*	*0.18186*	*0.83*	*13.22*	*2.51*	*0.94*	*2732*	*56*	*2670*	*14*	*103*
4.1	558	387	0.69	0.03	2.098	2.2	0.16840	0.27	11.07	2.23	0.99	2512	50	2541.8	4.5	99
6.2	543	309	0.57	0.02	2.126	2.2	0.16810	0.27	10.90	2.24	0.99	2495	49	2538.8	4.5	97
6.1	271	211	0.78	—	2.049	2.3	0.16792	0.40	11.30	2.35	0.99	2563	53	2537.0	6.7	101
4.2	1208	732	0.61	0.00	2.099	2.2	0.16772	0.18	11.02	2.25	1.0	2511	50	2535.0	3.1	99
22.1	*1503*	*1768*	*1.18*	*0.01*	*2.000*	*2.2*	*0.16672*	*0.16*	*11.50*	*2.21*	*1.0*	*2617*	*55*	*2524.9*	*2.7*	*104*
24.1	*1410*	*830*	*0.59*	*0.01*	*1.972*	*2.2*	*0.16640*	*0.16*	*11.64*	*2.24*	*1.0*	*2650*	*52*	*2521.8*	*2.6*	*106*
1.1	*1870*	*134*	*0.07*	*0.02*	*2.000*	*2.3*	*0.16484*	*0.15*	*11.36*	*2.26*	*1.0*	*2614*	*49*	*2506.0*	*2.5*	*105*
3.1	*2905*	*367*	*0.13*	*0.00*	*1.984*	*2.2*	*0.16343*	*0.11*	*11.36*	*2.21*	*1.0*	*2632*	*48*	*2491.4*	*1.9*	*107*
3.2	*2615*	*296*	*0.11*	*0.01*	*2.015*	*2.2*	*0.16156*	*0.13*	*11.05*	*2.21*	*1.0*	*2598*	*48*	*2472.1*	*2.1*	*106*
Domains with chaotic and blurry zoning																
5.1	136	89	0.65	0.13	2.116	2.3	0.16740	0.65	10.91	2.38	0.96	2501	51	2532	11	98
16.1	*148*	*101*	*0.68*	*0.01*	*2.110*	*2.5*	*0.16178*	*0.70*	*10.57*	*2.60*	*0.96*	*2502*	*59*	*2474*	*12*	*101*
5.2	*122*	*80*	*0.65*	*0.11*	*2.214*	*2.3*	*0.15835*	*0.71*	*9.864*	*2.40*	*0.95*	*2410*	*50*	*2438*	*12*	*98*
Analyses on mixtures of zones or cracked grain																
20.2	*134*	*80*	*0.59*	*0.08*	*1.832*	*2.3*	*0.18758*	*0.52*	*14.12*	*2.33*	*0.98*	*2815*	*55*	*2721.1*	*8.5*	*104*
31.1	*174*	*134*	*0.77*	*0.03*	*2.138*	*2.4*	*0.16322*	*0.53*	*10.52*	*2.41*	*0.98*	*2475*	*53*	*2489.3*	*8.9*	*99*

[a]Values corrected for common Pb.
[b]Percentage ^{206}Pb which is non-radiogenic.
[c]Error correlation between $^{238}U/^{206}Pb$ and $^{207}Pb/^{235}U$.
[d]Conc. (%): concordance = 100 (1 - $^{206}Pb/^{238}U$ /($e^{0.000155125a}$ −1)), where a is the $^{207}Pb/^{206}Pb$ age. Analyses in italics not used for concordia age.

Table 6
U–Th–Pb data for sample SMT03 from Mount Douglas.

Analysis					Ratios[a]							Ages[a]				
(Grain.spot)	U (ppm)	Th (ppm)	Th/U	$^{206}Pb_c$(%)[b]	$^{238}U/^{206}Pb$	±σ (%)	$^{207}Pb/^{206}Pb$	±σ (%)	$^{207}Pb/^{235}U$	±σ (%)	ρ[c]	$^{206}Pb/^{238}U$	±σ	$^{207}Pb/^{206}Pb$	±σ	Conc. (%)[d]
Well developed prisms, domains with oscilatory and sector zoning																
19.1	*678*	*304*	*0.45*	*0.01*	*1.867*	*2.4*	*0.18744*	*0.47*	*13.84*	*2.4*	*0.98*	*2765*	*56*	*2719.9*	*7.7*	*102*
12.1	*1270*	*374*	*0.29*	*0.01*	*1.771*	*2.2*	*0.18740*	*0.15*	*14.59*	*2.2*	*1.0*	*2892*	*53*	*2719.4*	*2.5*	*108*
17.1	*1079*	*694*	*0.64*	*0.01*	*1.796*	*2.4*	*0.18732*	*0.17*	*14.38*	*2.4*	*1.0*	*2857*	*60*	*2718.8*	*2.8*	*106*
12.2	*1340*	*133*	*0.10*	*0.01*	*1.888*	*2.2*	*0.18731*	*0.16*	*13.68*	*2.3*	*1.0*	*2742*	*51*	*2718.7*	*2.7*	*101*
14.2	*244*	*231*	*0.95*	—	*1.853*	*2.4*	*0.18628*	*0.64*	*13.86*	*2.5*	*0.97*	*2787*	*60*	*2710*	*10*	*103*
17.2	*845*	*398*	*0.47*	*0.02*	*1.906*	*2.2*	*0.18277*	*0.20*	*13.22*	*2.2*	*1.0*	*2723*	*52*	*2678.2*	*3.3*	*102*
14.1	*148*	*1232*	*8.31*	*0.02*	*1.593*	*2.3*	*0.17732*	*0.48*	*15.35*	*2.3*	*0.98*	*2531*	*23*	*2628.0*	*7.9*	*125*
4.1	319	288	0.90	0.03	1.988	2.4	0.1716	1.1	11.90	2.6	0.91	2634	57	2573	18	103
11.1	87	211	2.42	0.03	2.098	2.3	0.16940	0.80	11.13	2.5	0.95	2512	68	2552	13	98
13.1	316	223	0.71	0.04	2.028	2.2	0.16908	0.36	11.50	2.3	0.99	2589	51	2548.5	6.0	102
24.1	238	236	0.99	—	2.011	2.2	0.16884	0.47	11.58	2.3	0.98	2604	54	2546.1	7.8	103
22.2	67	45	0.67	0.13	2.031	2.4	0.16878	0.95	11.46	2.5	0.93	2580	54	2546	16	102
8.1	255	201	0.79	0.01	2.057	2.2	0.16789	0.42	11.25	2.3	0.98	2556	52	2536.7	7.1	101
10.1	406	370	0.91	0.03	2.112	2.2	0.16781	0.35	10.95	2.3	0.99	2511	51	2535.9	5.9	98
20.1	563	777	1.38	0.01	2.008	2.2	0.16750	0.27	11.50	2.2	0.99	2609	56	2532.8	4.5	103
29.2	181	148	0.82	0.01	2.057	2.3	0.16749	0.51	11.23	2.3	0.98	2559	52	2532.7	8.6	101
25.1	241	236	0.98	0.01	2.088	2.2	0.16717	0.44	11.04	2.3	0.98	2524	53	2529.5	7.5	100
16.1	411	453	1.10	0.00	2.008	2.2	0.16696	0.31	11.47	2.2	0.99	2610	54	2527.4	5.2	104
18.1	265	140	0.53	—	2.056	2.2	0.16676	0.42	11.19	2.3	0.98	2554	50	2525.4	7.0	101
21.1	123	120	0.98	—	2.045	2.3	0.16673	0.62	11.24	2.4	0.97	2570	54	2525	10	102
20.2	78	53	0.67	0.05	2.021	2.3	0.16671	0.87	11.37	2.5	0.94	2593	54	2525	15	103
29.1	344	410	1.19	0.02	2.053	2.2	0.16671	0.36	11.20	2.3	0.99	2563	55	2524.8	6.1	102
15.1	365	525	1.44	0.04	2.048	2.2	0.16659	0.33	11.22	2.3	0.99	2567	56	2523.7	5.5	102
26.1	336	472	1.40	0.01	1.971	2.3	0.16622	0.34	11.63	2.3	0.99	2645	59	2519.9	5.7	106
28.1	*1001*	*907*	*0.91*	*0.03*	*1.963*	*2.2*	*0.16619*	*0.19*	*11.67*	*2.2*	*1.0*	*2651*	*54*	*2519.7*	*3.2*	*107*
28.2	325	194	0.60	0.04	2.128	2.2	0.16589	0.41	10.75	2.3	0.98	2489	49	2516.6	6.8	98
15.2	*304*	*302*	*0.99*	*0.03*	*2.065*	*2.2*	*0.16567*	*0.39*	*11.06*	*2.3*	*0.99*	*2540*	*53*	*2514.4*	*6.5*	*102*
Domains with very weak or without visible zoning																
1.1	*60*	*19*	*0.33*	*0.09*	*1.888*	*2.8*	*0.18919*	*0.87*	*13.82*	*3.0*	*0.96*	*2740*	*65*	*2735*	*14*	*100*
9.1	*1053*	*246*	*0.23*	*0.01*	*1.837*	*2.2*	*0.18580*	*0.18*	*13.94*	*2.2*	*1.0*	*2801*	*51*	*2705.3*	*3.0*	*104*
27.1	359	109	0.30	0.01	1.995	2.2	0.17055	0.83	11.79	2.4	0.94	2618	50	2563	14	103
7.1	*666*	*482*	*0.72*	*0.00*	*1.987*	*2.3*	*0.16668*	*0.42*	*11.57*	*2.3*	*0.98*	*2629*	*54*	*2524.6*	*7.1*	*105*
27.2	*1090*	*11*	*0.01*	*0.03*	*1.986*	*2.2*	*0.16647*	*0.20*	*11.56*	*2.2*	*1.0*	*2629*	*48*	*2522.4*	*3.4*	*105*
6.2	*1733*	*18*	*0.01*	*0.01*	*1.994*	*2.2*	*0.16610*	*0.15*	*11.49*	*2.2*	*1.0*	*2620*	*48*	*2518.8*	*2.5*	*105*
6.1	*1110*	*177*	*0.16*	*0.02*	*1.997*	*2.2*	*0.16574*	*0.19*	*11.44*	*2.2*	*1.0*	*2618*	*49*	*2515.1*	*3.1*	*105*
5.1	*1326*	*18*	*0.01*	*0.00*	*2.016*	*2.3*	*0.16562*	*0.17*	*11.33*	*2.3*	*1.0*	*2597*	*48*	*2513.9*	*2.8*	*104*
19.2	*1623*	*583*	*0.36*	*0.01*	*2.088*	*2.2*	*0.16548*	*0.16*	*10.93*	*2.2*	*1.0*	*2525*	*48*	*2512.4*	*2.6*	*100*
31.1	*1893*	*19*	*0.01*	*0.00*	*2.005*	*2.2*	*0.16447*	*0.30*	*11.31*	*2.2*	*0.99*	*2608*	*48*	*2502.1*	*5.1*	*105*
30.1	406	152	0.38	0.01	2.100	2.2	0.16176	0.33	10.62	2.3	0.99	2512	48	2474.2	5.6	102
Rims																
26.2	407	148	0.36	0.02	2.037	2.4	0.16309	0.37	11.04	2.4	0.99	2578	53	2487.9	6.2	104
23.1	476	137	0.29	0.07	2.080	2.3	0.16305	0.31	10.81	2.3	0.99	2531	49	2487.5	5.2	102
28.3	678	183	0.27	0.35	2.069	2.3	0.16288	0.33	10.85	2.3	0.99	2549	50	2485.7	5.6	103
23.2	392	144	0.37	0.00	2.121	2.2	0.16228	0.34	10.55	2.3	0.99	2491	48	2479.6	5.7	101
Analyses on mixtures of zones																
13.2	*1111*	*24*	*0.02*	*0.02*	*1.981*	*2.2*	*0.16589*	*0.19*	*11.55*	*2.2*	*1.0*	*2635*	*48*	*2516.6*	*3.2*	*106*
10.2	*653*	*42*	*0.06*	*0.01*	*2.037*	*2.3*	*0.16507*	*0.26*	*11.17*	*2.3*	*0.99*	*2576*	*48*	*2508.3*	*4.3*	*103*

[a]Values corrected for common Pb.
[b]Percentage ^{206}Pb which is non-radiogenic.
[c]Error correlation between $^{238}U/^{206}Pb$ and $^{207}Pb/^{235}U$.
[d]Conc. (%): concordance = 100 (1 - $^{206}Pb/^{238}U$ /($e^{0.000155125a}$ −1)), where a is the $^{207}Pb/^{206}Pb$ age. Analyses in italics not used for concordia age.

Table 7
U–Th–Pb data for sample SMT05 from Gromov Nunataks.

Analysis					Ratios[a]							Ages[a]				
(Grain.spot)	U (ppm)	Th (ppm)	Th/U	$^{206}Pb_c$(%)[b]	$^{238}U/^{206}Pb$	±σ (%)	$^{207}Pb/^{206}Pb$	±σ (%)	$^{207}Pb/^{235}U$	±σ (%)	ρ[c]	$^{206}Pb/^{238}U$	±σ	$^{207}Pb/^{206}Pb$	±σ	Conc. (%)[d]
Oscillatory zoned domains																
24.2	*892*	*208*	*0.23*	*0.00*	*2.078*	*2.4*	*0.17321*	*0.41*	*11.50*	*2.4*	*0.98*	*2534*	*51*	*2588.9*	*6.9*	*97*
4.1	1466	381	0.26	0.01	2.035	2.4	0.1678	1.7	11.37	2.9	0.82	2578	52	2536	28	102
19.1	902	210	0.23	0.00	2.066	2.3	0.1670	1.1	11.14	2.5	0.91	2547	50	2527	18	101
5.2	1802	204	0.11	—	1.970	2.3	0.1666	1.1	11.66	2.6	0.90	2647	51	2524	19	106
9.3	1278	379	0.30	0.27	2.012	2.5	0.1662	2.5	11.39	3.5	0.70	2601	54	2519	43	104
3.1	*2025*	*406*	*0.20*	*0.01*	*1.991*	*2.4*	*0.16363*	*0.48*	*11.33*	*2.5*	*0.98*	*2626*	*54*	*2493.5*	*8.1*	*106*
5.1	*1601*	*602*	*0.38*	*0.00*	*2.078*	*2.3*	*0.16148*	*0.28*	*10.72*	*2.3*	*0.99*	*2534*	*50*	*2471.2*	*4.7*	*103*
11.2	*1190*	*304*	*0.26*	*0.00*	*2.038*	*2.2*	*0.16128*	*0.38*	*10.91*	*2.2*	*0.99*	*2573*	*48*	*2469.2*	*6.5*	*105*
9.1	*2515*	*728*	*0.29*	—	*1.974*	*2.3*	*0.16079*	*0.12*	*11.23*	*2.3*	*1.0*	*2641*	*50*	*2464.0*	*2.1*	*109*
8.1	*1684*	*433*	*0.26*	*0.01*	*2.029*	*2.3*	*0.16000*	*0.14*	*10.87*	*2.3*	*1.0*	*2584*	*50*	*2455.7*	*2.5*	*106*
9.2	*952*	*229*	*0.24*	*0.01*	*2.113*	*2.7*	*0.15995*	*0.22*	*10.44*	*2.7*	*1.0*	*2498*	*57*	*2455.1*	*3.8*	*102*
12.1	*1188*	*243*	*0.20*	*0.01*	*2.110*	*2.2*	*0.15993*	*0.18*	*10.45*	*2.2*	*1.0*	*2503*	*47*	*2454.9*	*3.1*	*102*
28.1	*1149*	*420*	*0.37*	*0.01*	*2.088*	*2.2*	*0.15955*	*0.51*	*10.54*	*2.3*	*0.97*	*2526*	*48*	*2450.9*	*8.5*	*104*
27.1	*1520*	*465*	*0.31*	*0.00*	*2.071*	*2.3*	*0.15825*	*0.51*	*10.54*	*2.4*	*0.98*	*2540*	*51*	*2437.1*	*8.6*	*105*
CL-dark cores without visible zoning																
7.1	2079	383	0.18	—	2.070	2.3	0.16752	0.51	11.16	2.4	0.98	2537	49	2533.0	8.6	100
16.1	1969	569	0.29	—	1.955	2.3	0.16580	0.36	11.69	2.3	0.99	2664	51	2515.7	6.1	107
13.1	*2947*	*533*	*0.18*	*0.00*	*1.982*	*2.2*	*0.1637*	*1.2*	*11.38*	*2.5*	*0.89*	*2634*	*49*	*2494*	*20*	*107*
23.1	*940*	*64*	*0.07*	—	*2.107*	*2.5*	*0.16240*	*0.71*	*10.63*	*2.6*	*0.96*	*2504*	*53*	*2481*	*12*	*101*
10.1	*2355*	*549*	*0.23*	*0.00*	*1.990*	*2.3*	*0.16067*	*0.12*	*11.13*	*2.3*	*1.0*	*2625*	*50*	*2462.7*	*2.1*	*108*
17.1	*1972*	*477*	*0.24*	*0.00*	*2.116*	*2.3*	*0.15970*	*0.68*	*10.41*	*2.4*	*0.96*	*2493*	*49*	*2452*	*12*	*102*
29.1	*1453*	*744*	*0.51*	*0.00*	*2.172*	*2.2*	*0.15763*	*0.18*	*10.01*	*2.2*	*1.0*	*2447*	*47*	*2430.4*	*3.0*	*101*
CL-bright domains without visible zoning																
2.1	*59*	*118*	*2.01*	*0.28*	*2.001*	*2.9*	*0.1669*	*1.7*	*11.50*	*3.4*	*0.87*	*2636*	*82*	*2526*	*28*	*104*
14.1	*81*	*166*	*2.04*	*0.10*	*2.115*	*2.3*	*0.16563*	*0.86*	*10.80*	*2.5*	*0.94*	*2500*	*64*	*2514*	*15*	*99*
18.1	*50*	*240*	*4.83*	*0.05*	*2.051*	*2.8*	*0.1625*	*1.4*	*10.93*	*3.1*	*0.90*	*2578*	*138*	*2482*	*23*	*104*
4.2	*173*	*307*	*1.78*	*0.07*	*2.064*	*2.6*	*0.16240*	*0.98*	*10.85*	*2.8*	*0.94*	*2567*	*70*	*2481*	*17*	*103*
15.2	*58*	*95*	*1.64*	*0.09*	*2.145*	*2.4*	*0.1586*	*1.1*	*10.20*	*2.7*	*0.91*	*2476*	*62*	*2440*	*19*	*101*
26.1	*58*	*194*	*3.36*	*0.23*	*2.172*	*2.4*	*0.1556*	*1.1*	*9.877*	*2.6*	*0.91*	*2459*	*82*	*2408*	*18*	*102*
Domain with chaotic zoning																
11.1	*491*	*185*	*0.38*	—	*2.164*	*2.3*	*0.15749*	*0.30*	*10.03*	*2.4*	*0.99*	*2446*	*50*	*2428.9*	*5.0*	*101*
Rims																
15.1	88	196	2.22	0.02	2.126	2.3	0.16043	0.75	10.40	2.4	0.95	2493	65	2460	13	101
18.2	49	105	2.13	0.07	2.116	2.4	0.1600	1.1	10.43	2.7	0.91	2499	67	2456	19	102
28.2	122	215	1.76	0.16	2.207	2.3	0.1586	1.4	9.907	2.7	0.85	2401	59	2441	24	98
6.1	39	46	1.19	1.15	2.131	2.5	0.1583	1.9	10.24	3.2	0.79	2493	61	2438	33	102
24.3	52	74	1.43	0.15	2.172	2.4	0.1582	1.2	10.04	2.7	0.89	2460	59	2437	20	100
1.2	18	7	0.38	0.95	2.072	2.8	0.1548	2.7	10.30	3.9	0.72	2550	60	2399	46	107
22.2	*56*	*102*	*1.82*	*1.24*	*2.241*	*2.9*	*0.1504*	*1.5*	*9.252*	*3.3*	*0.88*	*2401*	*73*	*2350*	*26*	*101*
Analyses on mixtures of zones																
1.1	*1517*	*102*	*0.07*	*0.01*	*1.917*	*2.4*	*0.1746*	*1.1*	*12.56*	*2.7*	*0.91*	*2708*	*54*	*2602*	*18*	*105*
21.1	*1975*	*189*	*0.10*	*0.02*	*2.050*	*2.4*	*0.16624*	*0.95*	*11.18*	*2.6*	*0.93*	*2562*	*51*	*2520*	*16*	*102*
30.1	*1373*	*635*	*0.46*	*0.01*	*2.089*	*2.3*	*0.16400*	*0.17*	*10.83*	*2.3*	*1.00*	*2523*	*51*	*2497.4*	*2.8*	*101*
20.1	*1474*	*238*	*0.16*	*0.01*	*2.077*	*2.2*	*0.16273*	*0.16*	*10.80*	*2.2*	*1.00*	*2535*	*47*	*2484.2*	*2.8*	*102*
25.1	*1684*	*384*	*0.23*	*0.01*	*2.033*	*2.2*	*0.16188*	*0.53*	*10.98*	*2.3*	*0.97*	*2580*	*48*	*2475.3*	*9.0*	*105*
29.2	*1313*	*116*	*0.09*	*0.02*	*2.131*	*2.2*	*0.16185*	*0.46*	*10.47*	*2.3*	*0.98*	*2481*	*47*	*2475.1*	*7.7*	*100*
24.1	*737*	*184*	*0.25*	*0.05*	*2.123*	*2.8*	*0.15997*	*0.25*	*10.39*	*2.9*	*1.00*	*2490*	*60*	*2455.4*	*4.2*	*102*
22.1	*827*	*301*	*0.36*	*0.00*	*2.234*	*2.3*	*0.1598*	*1.1*	*9.865*	*2.6*	*0.91*	*2388*	*48*	*2454*	*18*	*97*

[a]Values corrected for common Pb.
[b]Percentage ^{206}Pb which is non-radiogenic.
[c]Error correlation between $^{238}U/^{206}Pb$ and $^{207}Pb/^{235}U$.
[d]Conc. (%): concordance = 100 (1 - $^{206}Pb/^{238}U$ /($e^{0.000155125a}$ −1)), where a is the $^{207}Pb/^{206}Pb$ age. Analyses in italics not used for concordia age.

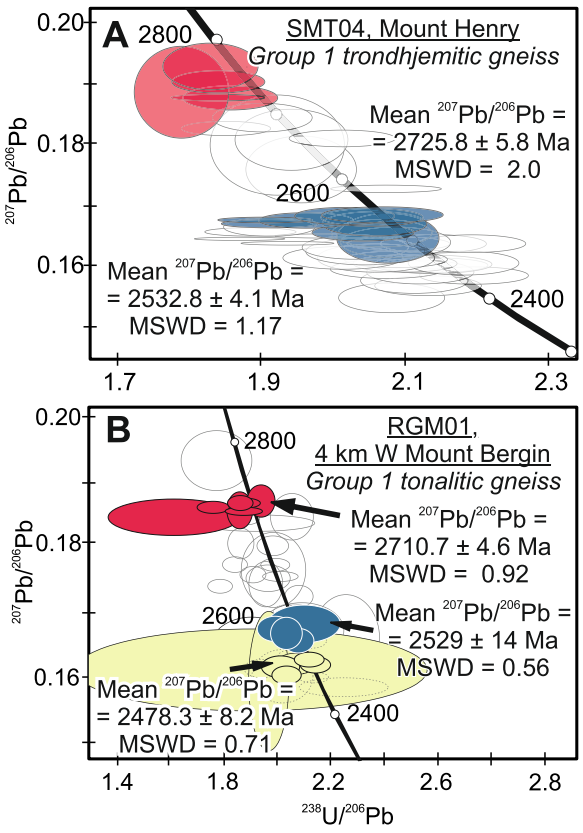

Fig. 7. Tera-Wasserburg concordia diagrams of zircon U-Pb analyses of *Group 1* orthogneisses from the Scott and Raggatt Mountains. A – SMT04. B – RGM01. Error ellipses are 1 sigma. Ages along the concordia are in Ma.

ca. 2.7 Ga for trondhjemitic gneiss from Mt. Henry (SMT04) and for a tonalitic gneiss, 3 km west of Mount Bergin (RMG01). Both samples belong to geochemical *Group 1*. The age estimates from these two samples are considerably older than those from Tonagh Island. Ages of *ca.* 2750–2700 Ma were also found in inherited/xenocrystic cores from the two youngest samples from Mt. Douglas (SMT02 and SMT03), which belong to geochemical *Group 2*. One gneiss from Mt. Douglas has older inherited/xenocrystic cores with an age of *ca.* 2.9 Ga. This is similar to the ages of protoliths to orthogneisses from the Tula Mountains (Kelly and Harley, 2005; Król et al., 2020).

6.2.2. *Circa 2.5 Ga magmatic and metamorphic ages*

It has been well established that high-temperature metamorphism occurred in the Napier Complex between 2585 and 2420 Ma (Harley, 2016; Clark et al., 2018; Harley et al., 2019 and references therein; Król et al., 2020; Kusiak et al., 2021). This study adds to the known extent of this event, with ages of 2533 ± 4 Ma at Mt. Henry and 2529 ± 14 Ma at nearby Mt. Bergin, from metamorphic zircon in gneisses with *ca.* 2720 Ma protoliths. These ages overlap those for magmatic protoliths from the Scott Mountains (≥2533 ± 5 Ma and 2539 ± 5 Ma at Mt. Douglas and ≥2522 ± 9 Ma at Gromov Nunataks). The *ca.* 2530 Ma ages for protoliths to orthogneiss have not been found in previous studies on the Napier Complex. However, they are present in detrital zircon with magmatic growth zoning from paragneiss samples at Fyfe Hills (Takehara et al., 2020).

Many authors have highlighted the prolonged nature of the *ca.* 2.5 Ga HT-UHT metamorphism in the Napier Complex (*e.g.,* Harley and Black, 1987; Carson et al., 2002a,b; Kelly and Harley, 2005; Suzuki et al., 2006; Clark et al., 2018). Within this period, there is evidence for distinct episodes of zircon growth before and after 2500 Ma, with most of the data ranging in two groups from 2550 to 2510 Ma and 2490–2460

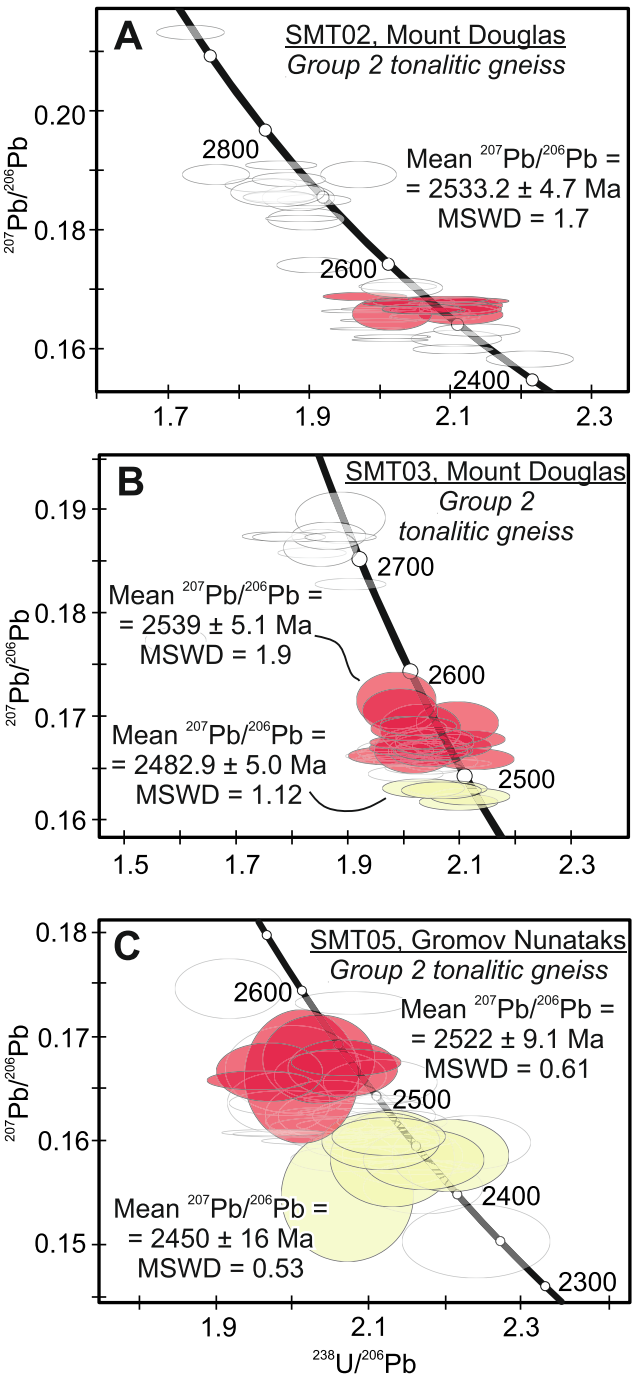

Fig. 8. Tera-Wasserburg concordia diagrams of zircon U-Pb analyses of *Group 2* orthogneisses from the Scott and Raggatt Mountains. A – SMT02. B – SMT03. C – SMT05. Error ellipses are 1 sigma. Ages along the concordia are in Ma.

Ma, as shown in Fig. 10. This is also the case in the Scott and Raggatt Mountain ranges. For example, in the sample from Mt. Bergin, the older zircon population is mostly U-rich with Th/U < 0.1, whereas zircon of *ca.* 2.48 Ga has lower U and Th/U > 1. Two sets of metamorphic zircon ages and geochemical compositions within the *ca.* 2.5 Ga event have also been observed in individual samples from the Tula Mountains (*e.g.,* Mount King, Król et al., 2020). A thermal peak of metamorphism at *ca.* 2.48 Ga has been suggested by Hokada et al. (2003) and Grew et al. (2006) to explain younger ages of metamorphic zircon. In contrast, Harley (2016) suggested that the later stage of zircon growth postdates the thermal (UHT) peak of metamorphism, and instead can be attributed to zircon growth during cooling and/or interaction between anatectic

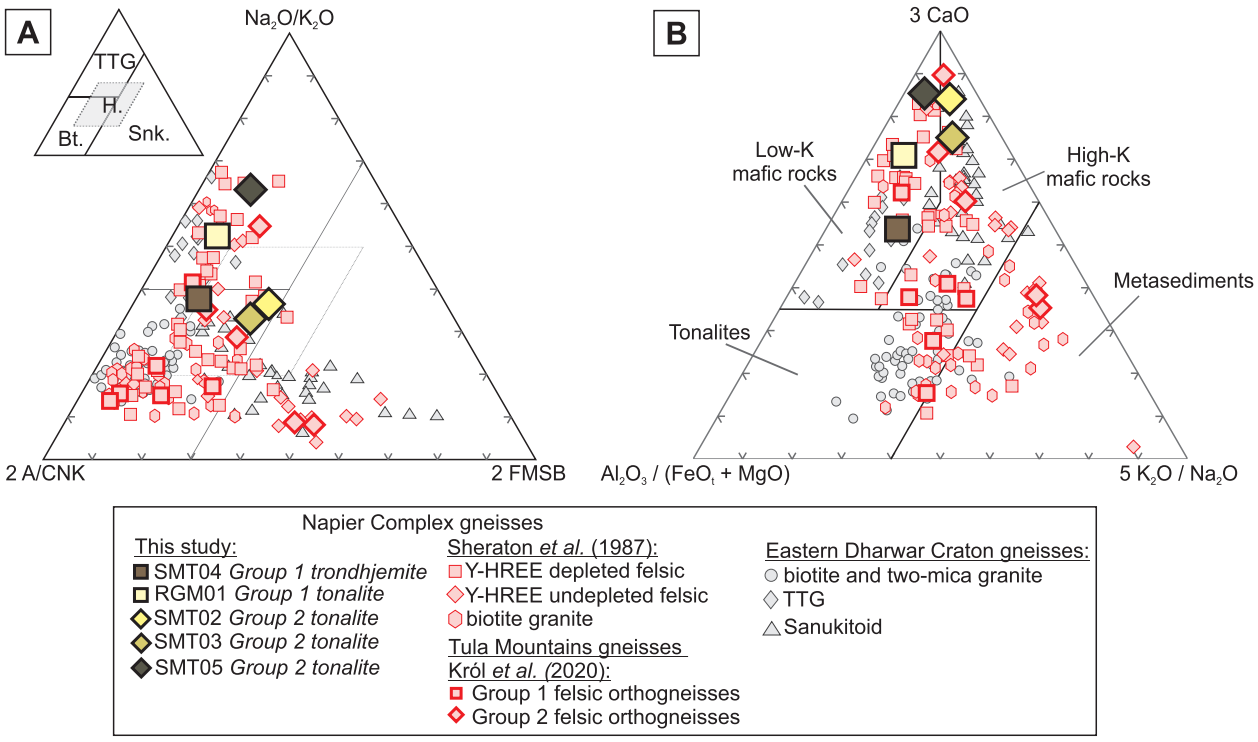

Fig. 9. A –Ternary classification diagram for late Archean granitoids (Laurent et al., 2014): 2A/CNK = 2 * molar $Al_2O_3/(CaO + Na_2O + K_2O$ ratio). 2FMSB = 2 * $(FeOt + MgO)_{wt.\%}$ * $(Sr + Ba)_{wt.\%}$. Fields of late Archean granitoids (inset): TTG = tonalite-trondhjemite-granodiorite; Snk. = sanukitoids *sensu lato*; Bt. γ = biotite- and two-mica granites; H. – hybrid). B – Ternary classification diagram Al_2O_3 / $(FeO_t + MgO) - 3 \times CaO - 5 \times (K_2O/Na_2O)$ with the fields representing the source types for granitoid melts (Laurent et al., 2014). Data sources as in Fig. 3.

melt and wall rocks. Alternatively, the data in this study and in Król et al. (2020) may indicate thermal pulses within an extended metamorphic event.

The Th/U ratio has been widely used to distinguish metamorphic from igneous zircon (Hoskin and Black, 2000), although such differences are not systematic, and high Th/U zircon has been recognized in many high-grade metamorphic rocks (*e.g.,* Hokada et al., 2004; Kelly and Harley, 2005; Santosh et al., 2007; Król et al., 2020). The differences in Th/U in metamorphic zircon can be ascribed to the presence or absence of certain minerals or phases (*e.g.,* melt) that partition Th over U, especially monazite and allanite (Rubatto, 2017; Yakymchuk et al., 2018).

This study recognizes magmatic tonalitic protoliths crystallizing at or shortly before 2530 Ma. These are the youngest Neoarchean protoliths to orthogneisses recognized in the Napier Complex and crystallized during the window of metamorphism defined by Harley (2016). As such, they may be an indication of episodes of heating and cooling within a broader metamorphic event. Alternatively, *ca.* 2530 Ma tonalitic protoliths can be a product of partial melting of metabasites within the orogen (Harley, 1989, 1992; Johnson et al., 2012; Palin et al., 2016) during HT metamorphism. Apparent coevality of zircon crystallisation from melt at Mount Bergin and Mount Henry, and growth of metamorphic zircon at Mount Douglas and Gromov Nunatak, can be reconciled by the spatial variability in the temperature and volume of the orogen. During high-grade metamorphism melt can be effectively extracted and transferred (*e.g.,* Brown, 2013). The transfer of melt may occur in pulses (Brown, 2013) and on various scales so that local cross-cutting relations (*e.g.,* deformation markers, melt veining, dykes) do not upscale to larger regions (Marchildon and Brown, 2003). The melt eventually crystalizes as a consequence of temperature drop and/or by loss of H_2O. The process of melt loss during (ultra) high-temperature metamorphism has been identified in many other high-grade terranes (for example Fyfe, 1973; Waters, 1988; White and Powell, 2002; Johnson et al., 2012; Palin et al., 2016; White et al., 2017). The inferred pressures of <1.2 GPa for generation of *ca.* 2530 Ma tonalitic melts agree with the pressures of high-grade metamorphism in the Napier Complex (0.7–1.1 GPa, Ellis, 1980; Harley and Motoyoshi, 2000; Hokada et al., 2008) and many granulitic terranes elsewhere (Harley, 1992 and references therein).

6.3. *Implications for the crustal evolution in the Napier Complex*

Across the Napier Complex, different areas contain orthogneisses that have yielded different U-Pb zircon ages for their magmatic protoliths (Fig. 10). Orthogneisses with protolith ages of 3.3–2.9 Ga show evidence of high-T/low-P metamorphism at *ca.* 2.8 Ga (Harley and Black, 1997; Hokada et al., 2003; Kelly and Harley, 2005; Król et al., 2020). In contrast, no *ca.* 2.8 Ga metamorphic event has been documented in rocks with >3.5 Ga protoliths. Rocks from the southwestern Napier Complex, including the southern Scott Mountains and Raggatt Mountains, Fyfe Hills, and Tonagh Island, record igneous activity between 2750 and 2620 Ma (Carson et al., 2002a; Crowe et al., 2002; Horie et al., 2012; present study). In the absence of zircon Hf isotope data, it is unknown how much of this magmatism has resulted from remelting of pre-existing continental crust. Nevertheless, in contrast to *Group 1*, *ca.* 2.72 Ga tonalitic-trondhjemitic gneisses that lack inherited/xenocrystic zircon, two *ca.* 2.53 Ga *Group 2* gneisses from Mount Douglas show considerable incorporation of *ca.* 2.7 Ga material (Fig. 8). Evidence for the involvement of crust older than 2.8 Ga is provided by a whole-rock Rb-Sr age for a charnockite from Fyfe Hills ($3120^{+230}/_{-180}$ Ma, Black et al., 1983b) and by a whole-rock Sm-Nd age for a mafic gneiss from Tonagh Island (3708 ± 53 Ma, Owada et al., 1994). This is confirmed by $Nd(t)_{DM}$ model ages from these samples (Shiraishi et al., 2008). However, the involvement of older crust in the southern Scott and Raggatt Mountains has not been established, although there is one concordant *ca.* 2.9 Ga age from Mount Douglas (this study), similar to a discordant >2.9 Ga zircon from Fyfe Hills (Black et al., 1983b).

The *ca.* 2.72 Ga magmatism in the southern Scott and Raggatt

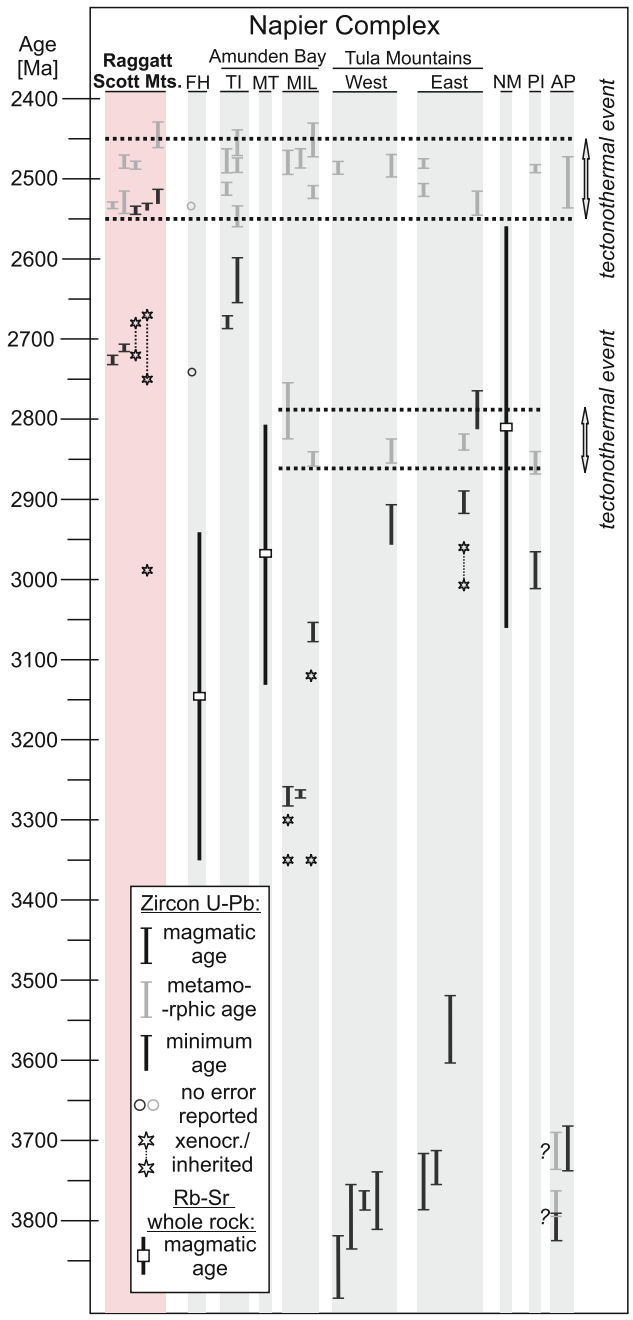

Fig. 10. Comparison of U-Pb igneous and metamorphic ages for orthogneisses from the Napier Complex. Data sources: AP – Aker Peaks: Kusiak et al. (2021); FH – Fyfe Hills: Black et al. (1983b), Horie et al. (2012); MIL – Mount Riiser-Larsen: Hokada et al. (2003); MT – Mount Tod: Black et al. (1983b); NM – Napier Mountains: Black et al. (1986a); PI – Proclamation Island: Kelly and Harley (2005); SR Mts. – Scott and Raggatt Mountains: this study; TI – Tonagh Island: Carson et al. (2002a); Crowe et al. (2002); Tula Mountains West: Harley and Black (1997); Kelly and Harley (2005); Kusiak et al. (2013a), Guitreau et al. (2019); Tula Mountains East: Król et al. (2020).

Mountains was generated at high pressures (>1.5 GPa), postdating the *ca.* 2.8 Ga tectonothermal event in the Tula Mountains, at Mt Riiser-Larsen, and further north on Proclamation Island. It is unclear whether this represents crustal growth at the margin of a pre-existing *ca.* 2.8 Ga continent, or whether it independently developed in a magmatic arc that was later juxtaposed.

Following the chronology presented in Sheraton et al. (1987), Kelly and Harley (2005) proposed that the Napier Complex has been a single entity since *ca.* 2850 Ma. However, only the *ca.* 2.5 Ga tectonothermal event is recorded across the entire Napier Complex (Fig. 10), indicating that the complex may not have been an entity before this time. The possibility that there may be several crustal blocks within the Napier Complex remains a perplexing question that can only be tested by further dating of orthogneisses from across the entire Napier Complex.

7. Conclusions

The recognition of the widespread *ca.* 2720 Ma igneous event in the Scott and Raggatt Mountains is established by protolith ages from tonalitic (3 km west of Mount Bergin) and trondhjemitic (Mount Henry) orthogneiss and xenocrystic/inherited zircon from two tonalitic gneisses from Mount Douglas. The geochemistry of the *ca.* 2720 Ma rocks implies that their formation involved melting of basaltic crust under pressures of at least 1.5 GPa. Subsequent *syn*-metamorphic *ca.* 2530 Ma tonalitic magmatism was generated at lower pressures.

All these rocks post-date the *ca.* 2.8 Ga metamorphic event recognized in many Napier Complex orthogneisses with protolith ages of 3.3–2.9 Ga. Furthermore, no *ca.* 2.8 Ga metamorphic event has been documented in rocks with >3.5 Ga protoliths. The presence of granitoid protoliths emplaced during the 2585–2420 Ma tectonothermal event, as now established for the Scott and Raggatt Mountains, indicates partial melting during ultra-high temperature metamorphism. When these results are evaluated against the known, albeit sparse, protolith ages from across the Napier Complex, it also raises the possibility that the complex likely contains crustal domains of different ages and origins that may not have been assembled until the major *ca.* 2.5 Ga tectonothermal event.

CRediT authorship contribution statement

Piotr Król: Conceptualization, Formal analysis, Investigation, Methodology, Visualization, Writing – original draft, Writing – review & editing. **Monika A. Kusiak:** Conceptualization, Data curation, Formal analysis, Funding acquisition, Investigation, Methodology, Resources, Supervision, Writing – review & editing. **Daniel J. Dunkley:** Conceptualization, Resources, Writing – review & editing. **Simon A. Wilde:** Conceptualization, Funding acquisition, Writing – review & editing. **Keewook Yi:** Formal analysis, Methodology, Validation. **Martin J. Whitehouse:** Writing – review & editing. **Shinae Lee:** Formal analysis, Validation. **Simon L. Harley:** Writing – review & editing.

Declaration of Competing Interest

The authors declare that they have no known competing financial interests or personal relationships that could have appeared to influence the work reported in this paper.

Acknowledgements

The research leading to these results has received funding from the Norwegian Financial Mechanism 2014-2021: UMO2019/34/H/ST10/00619 to MAK; Australian Antarctic Science Grant: Project No. 4548 to SAW; and was supported by KBSI under the R&D program (Project No. D37700) supervised by the Ministry of Science and ICT, South Korea. Chris Carson and Alix Post of Geoscience Australia are thanked for help, discussion, and especially for access to legacy samples collected by the Bureau of Mineral Resources during Australian National Antarctic Research Expeditions. Two anonymous reviewers are thanked for their comment, which assisted us in improving the manuscript.

References

Asami, M., Suzuki, K., Grew, E.S., 2002. Chemical Th-U-total Pb dating by electron microprobe analysis of monazite, xenotime and zircon from the Archean Napier complex, East Antarctica: Evidence for ultra-high-temperature metamorphism at

2400 Ma. Precambr. Res. 114 (3-4), 249–275. https://doi.org/10.1016/S0301-9268(01)00228-5.
Balakrishnan, S., Rajamani, V., 1987. Geochemistry and petrogenesis of granitoids around the Kolar Schist Belt, south India: constraints for the evolution of the crust in the Kolar area. J. Geol. 95 (2), 219–240. https://doi.org/10.1086/629121.
Barker, F., 1979. Trondhjemite: Definition, environment and hypotheses of origin. In: Barker, F. (Ed.), Trondhjemites, Dacites, and Related Rocks. Elsevier, pp. 1–12. https://doi.org/10.1016/B978-0-444-41765-7.50006-X.
Barker, F., Arth, J.G., 1976. Generation of trondhjemitic-tonalitic liquids and Archaean bimodal trondhjemitie-basalt suites. Geology 4, 596–600. https://doi.org/10.1130/0091-7613(1976)4<596.
Belyatsky, B.V., Rodionov, N.V., Antonov, A.V., Sergeev, S.A., 2011. The 3.98–3.63 Ga zircons as indicators of major processes operating in the ancient continental crust of the east Antarctic shield (Enderby Land). Dokl. Earth Sci. 438 (2), 770–774. https://doi.org/10.1134/S1028334X11060031.
Bhaskar Rao, Y., Sivaraman, T., Pantulu, G., Gopalan, K., Naqvi, S., 1992. Rb-Sr ages of late Archean metavolcanics and granites, Dharwar craton, South India and evidence for Early Proterozoic thermotectonic event(s). Precambr. Res. 59 (1–2), 145–170. https://doi.org/10.1016/0301-9268(92)90055-S.
Black, L.P., Fitzgerald, J.D., Harley, S.L., 1984. Pb isotopic composition, colour, and microstructure of monazites from a polymetamorphic rock in Antarctica. Contrib. Mineral. Petrol. 85 (2), 141–148. https://doi.org/10.1007/BF00371704.
Black, L.P., James, P.R., Harley, S.L., 1983a. Geochronology and geological evolution of metamorphic rocks in the Field Islands area, East Antarctica. J. Metamorph. Geol. 1 (4), 277–303. https://doi.org/10.1111/j.1525-1314.1983.tb00276.x.
Black, L.P., James, P.R., Harley, S.L., 1983b. The geochronology, structure and metamorphism of early Archean rocks at Fyfe Hills, Enderby Land, Antarctica. Precambrian Res. 21 (3–4), 197–222. https://doi.org/10.1016/0301-9268(83)90041-4.
Black, L.P., Sheraton, J.W., James, P.R., 1986a. Late Archaean granites of the Napier Complex, Enderby Land, Antarctica: A comparison of Rb-Sr, Sm-Nd and U-Pb isotopic systematics in a complex terrain. Precambr. Res. 32 (4), 343–368. https://doi.org/10.1016/0301-9268(86)90036-7.
Black, L.P., Williams, I.S., Compston, W., 1986b. Four zircon ages from one rock: the history of a 3930 Ma-old granulite from Mount Sones, Enderby Land, Antarctica. Contrib. Mineral. Petrol. 94 (4), 427–437. https://doi.org/10.1007/BF00376336.
Brown, M., 2013. Granite: From genesis to emplacement. Bull. Geol. Soc. Am. 125 (7-8), 1079–1113. https://doi.org/10.1130/B30877.1.
Carson, C.J., Ague, J.J., Coath, C.D., 2002a. U-Pb geochronology from Tonagh Island, East Antarctica: Implications for the timing of ultra-high temperature metamorphism of the Napier Complex. Precambr. Res. 116 (3–4), 237–263. https://doi.org/10.1016/S0301-9268(02)00023-2.
Carson, C.J., Ague, J.J., Grove, M., Coath, C.D., Harrison, T.M., 2002b. U-Pb isotopic behaviour of zircon during upper-amphibolite facies fluid infiltration in the Napier Complex, East Antarctica. Earth Planet. Sci. Lett. 199 (3-4), 287–310. https://doi.org/10.1016/S0012-821X(02)00565-4.
Corfu, F., Hanchar, J.M., Hoskin, P.W.O., Kinny, P., 2003. Atlas of zircon textures. Rev. Mineral. Geochemistry 53, 469–500. https://doi.org/10.2113/0530469.
Clark, C., Taylor, R.J.M., Kylander-Clark, A.R.C., Hacker, B.R., 2018. Prolonged (>100 Ma) ultrahigh temperature metamorphism in the Napier Complex, East Antarctica: A petrochronological investigation of Earth's hottest crust. J. Metamorph. Geol. 36, 1117–1139. https://doi.org/10.1111/jmg.12430.
Crowe, W.A., Osanai, Y., Toyoshima, T., Owada, M., Tsunogae, T., Hokada, T., 2002. SHRIMP geochronology of a mylonite zone on Tonagh Island: characterisation of the last high-grade tectonothermal event in the Napier Complex, East Antarctica. Polar Geosci. 15, 17–36. https://doi.org/10.15094/00003106.
Defant, M.J., Drummond, M.S., 1990. Derivation of some modern arc magmas by melting of young subducted lithosphere. Nature 347, 662–665. https://doi.org/10.1038/347662a0.
Dey, S., Gajapathi Rao, R., Gorikhan, R.A., Veerabhaskar, D., Kumar, S., Kumar, M.K., 2003. Geochemistry and origin of Northern Closepet Granite from Gudur-Guledagudda area, Bagalkot District, Karnataka. J. Geol. Soc. India 62, 152–168.
Dey, S., Nandy, J., Choudhary, A.K., Liu, Y., Zong, K., 2014. Origin and evolution of granitoids associated with the Kadiri greenstone belt, eastern Dharwar craton: A history of orogenic to anorogenic magmatism. Precambr. Res. 246, 64–90. https://doi.org/10.1016/j.precamres.2014.02.007.
Dey, S., Pandey, U.K., Rai, A.K., Chaki, A., 2012. Geochemical and Nd isotope constraints on petrogenesis of granitoids from NW part of the eastern Dharwar craton: Possible implications for late Archaean crustal accretion. J. Asian Earth Sci. 45, 40–56. https://doi.org/10.1016/j.jseaes.2011.09.013.
Dey, S., Rai, A.K., Chaki, A., 2009. Geochemistry of granitoids of Bilgi area, northern part of eastern Dharwar craton, southern India - Example of transitional TTGs derived from depleted source. J. Geol. Soc. India 73 (6), 854–870. https://doi.org/10.1007/s12594-009-0068-y.
Ellis, D.J., 1980. Osumilite-sapphirine-quartz granulites from Enderby Land, Antarctica: P-T conditions of metamorphism, implications for garnet-cordierite equilibria and the evolution of the deep crust. Contrib. Mineral. Petrol. 74 (2), 201–210. https://doi.org/10.1007/BF01132005.
Fitzsimons, I.C.W., 2000. A review of tectonic events in the East Antarctic Shield and their implications for Gondwana and earlier supercontinents. J. Afr. Earth Sc. 31 (1), 3–23. https://doi.org/10.1016/S0899-5362(00)00069-5.
Fyfe, W.S., 1973. A discussion on the evolution of the Precambrian crust - the granulite facies, partial melting and the Archaean crust. T. Roy. Soc. Lond. A. 273, 457–461.
Gagnevin, D., Daly, J.S., Kronz, A., 2010. Zircon texture and chemical composition as a guide to magmatic processes and mixing in a granitic environment and coeval volcanic system. Contrib. Mineral. Petrol. 159 (4), 579–596. https://doi.org/10.1007/s00410-009-0443-0.
Grew, E.S., Manton, W.I., 1979. Archean Rocks in Antarctica: 2.5-Billion-Year Uranium-Lead Ages of Pegmatites in Enderby Land. Science 206 (4417), 443–445.
Grew, E.S., Yates, M.G., Shearer, C.K., Hagerty, J.J., Sheraton, J.W., Sandiford, M., 2006. Beryllium and other trace elements in paragneisses and anatectic veins of the ultrahigh-temperature Napier complex, Enderby land, East Antarctica: The role of sapphirine. J. Petrol. 47, 859–882. https://doi.org/10.1093/petrology/egi098.
Guitreau, M., Boyet, M., Paquette, J.-L., Gannoun, A., Konc, Z., Benbakkar, M., Suchorski, K., Hénot, J.-M., 2019. Hadean protocrust reworking at the origin of the Archean Napier Complex (Antarctica). Geochem. Perspect. Lett. 12, 7–11. https://doi.org/10.7185/geochemlet.1927.
Halla, J., 2018. Highlights on Geochemical Changes in Archaean Granitoids and Their Implications for Early Earth Geodynamics. Geosciences 8 (9), 353. https://doi.org/10.3390/geosciences8090353.
Halla, J., van Hunen, J., Heilimo, E., Hölttä, P., 2009. Geochemical and numerical constraints on Neoarchean plate tectonics. Precambr. Res. 174 (1-2), 155–162. https://doi.org/10.1016/j.precamres.2009.07.008.
Harley, S.L., 1985. Garnet-Orthopyroxene Bearing Granulites from Enderby Land, Antarctica: Metamorphic Pressure-Temperature-Time Evolution of the Archaean Napier Complex. J. Petr. 26 (4), 819–856. https://doi.org/10.1093/petrology/26.4.819.
Harley, S.L., 1989. The origins of granulites: A metamorphic perspective. Geol. Mag. 126 (3), 215–247. https://doi.org/10.1017/S0016756800022330.
Harley, S.L., 1992. Proterozoic granulite terranes. In: Condie, K.C. (Ed.), Developments in Precambrian Geology, vol. 10. Elsevier, pp. 301–359. https://doi.org/10.1016/S0166-2635(08)70122-1.
Harley, S.L., 2016. A matter of time: The importance of the duration of UHT metamorphism. J. Mineral. Petrol. Sci. 111 (2), 50–72. https://doi.org/10.2465/jmps.160128.
Harley, S.L., Black, L.P., 1987. The Archaean geological evolution of Enderby Land, Antarctica. Geol. Soc. Lond. Spec. Publ. 27 (1), 285–296. https://doi.org/10.1144/GSL.SP.1987.027.01.24.
Harley, S.L., Black, L.P., 1997. A revised Archaean chronology for the Napier Complex, Enderby Land, from SHRIMP ion-microprobe studies. Antarct. Sci. 9 (1), 74–91. https://doi.org/10.1017/S0954102097000102.
Harley, S.L., Fitzsimons, I.C.W., Zhao, Y., 2013. Antarctica and supercontinent evolution: Historical perspectives, recent advances and unresolved issues. Geol. Soc. Lond. Spec. Publ. 383 (1), 1–34. https://doi.org/10.1144/SP383.9.
Harley, S.L., Hensen, B.J., Sheraton, J.W., 1990. Two-stage decompression in orthopyroxene-sillimanite granulites from Forefinger Point, Enderby land, Antarctica: implications for the evolution of the Archaean Napier Complex. J. Metamorph. Geol. 8 (6), 591–613. https://doi.org/10.1111/j.1525-1314.1990.tb00490.x.
Harley, S.L., Kelly, N.M., Kusiak, M.A., 2019. Ancient Antarctica: The Archean of the East Antarctic Shield. In: van Kranendonk, M.J., Bennett, V.C., Hoffmann, J.E. (Eds.), Earth's Oldest Rocks (Second Edition). Elsevier, pp. 856–897.
Harley, S.L., Motoyoshi, Y., 2000. Al zoning in orthopyroxene in a sapphirine quartzite: Evidence for >1120 °C UHT metamorphism in the Napier Complex, Antarctica, and implications for the entropy of sapphirine. Contrib. Mineral. Petrol. 138, 293–307. https://doi.org/10.1007/s004100050564.
Harley, S.L., Nandakumar, V., 2014. Accessory Mineral Behaviour in Granulite Migmatites: a Case Study from the Kerala Khondalite Belt, India. J. Petrol. 55, 1965–2002. https://doi.org/10.1093/petrology/egu047.
Hiess, J., Bennett, V.C., 2016. Chondritic Lu/Hf in the early crust-mantle system as recorded by zircon populations from the oldest Eoarchean rocks of Yilgarn Craton, West Australia and Enderby Land, Antarctica. Chem. Geol. 427, 125–143. https://doi.org/10.1016/j.chemgeo.2016.02.011.
Hokada, T., Misawa, K., Shiraishi, K., Suzuki, S., 2003. Mid to late Archaean (3.3-2.5 Ga) tonalitic crustal formation and high-grade metamorphism at Mt. Riiser-Larsen, Napier Complex, East Antarctica. Precambrian Res. 127 (1-3), 215–228. https://doi.org/10.1016/S0301-9268(03)00188-8.
Hokada, T., Misawa, K., Yokoyama, K., Shiraishi, K., Yamaguchi, A., 2004. SHRIMP and electron micropobe chronology of UHT metamorphism in the Napier Complex, East Antarctica: Implications for zircon growth at 1,000 °C. Contrib. Mineral. Petrol. 147, 1–20. https://doi.org/10.1007/s00410-003-0550-2.
Hokada, T., Motoyoshi, Y., Suzuki, S., Ishikawa, M., Ishizuka, H., 2008. Geodynamic evolution of Mt. Riiser-Larsen, Napier Complex, East Antarctica, with reference to the UHT mineral associations and their reaction relations. Geol. Soc. Lond. Spec. Publ. 308 (1), 253–282. https://doi.org/10.1144/SP308.13.
Horie, K., Hokada, T., Hiroi, Y., Motoyoshi, Y., Shiraishi, K., 2012. Contrasting Archaean crustal records in western part of the Napier Complex, East Antarctica: New constraints from SHRIMP geochronology. Gondwana Res. 21 (4), 829–837. https://doi.org/10.1016/j.gr.2011.08.013.
Hoskin, P.W.O., Black, L.P., 2000. Metamorphic zircon formation by solid-state recrystallization of protolith igneous zircon. J. Metamorph. Geol. 18 (4), 423–439. https://doi.org/10.1046/j.1525-1314.2000.00266.x.
Jahn, B.-M., Glikson, A.Y., Peucat, J.J., Hickman, A.H., 1981. REE geochemistry and isotopic data of Archean silicic volcanics and granitoids from the Pilbara Block, Western Australia: implications for the early crustal evolution. Geochim. Cosmochim. Acta 45 (9), 1633–1652. https://doi.org/10.1016/S0016-7037(81)80002-6.
Janoušek, V., Moyen, J.F., Martin, H., Erban, V., Farrow, C., 2016. Geochemical Modelling of Igneous Processes – Principles And Recipes in R Language. Springer-Verlag, Berlin Heidelberg.

Jayananda, M., Martin, H., Peucat, J.-J., Mahabaleswar, B., 1995. Late Archaean crust-mantle interactions: geochemistry of LREE-enriched mantle derived magmas. Example of the Closepet batholith, southern India. Contrib. Mineral. Petrol. 119 (2-3), 314–329. https://doi.org/10.1007/BF00307290.

Jayananda, M., Moyen, J.-F., Martin, H., Peucat, J.-J., Auvray, B., Mahabaleswar, B., 2000. Late Archaean (2550–2520 Ma) juvenile magmatism in the Eastern Dharwar craton, southern India: Constraints from geochronology, Nd-Sr isotopes and whole rock geochemistry. Precambr. Res. 99 (3-4), 225–254. https://doi.org/10.1016/S0301-9268(99)00063-7.

Johnson, T.E., Brown, M., Gardiner, N.J., Kirkland, C.L., Smithies, R.H., 2017. Earth's first stable continents did not form by subduction. Nature 543 (7644), 239–242. https://doi.org/10.1038/nature21383.

Johnson, T.E., Fischer, S., White, R.W., Brown, M., Rollinson, H.R., 2012. Archaean intracrustal differentiation from partial melting of metagabbro-field and geochemical evidence from the central region of the Lewisian complex, NW Scotland. J. Petrol. 53 (10), 2115–2138. https://doi.org/10.1093/petrology/egs046.

Kelly, N.M., Harley, S.L., 2005. An integrated microtextural and chemical approach to zircon geochronology: Refining the Archaean history of the Napier Complex, east Antarctica. Contrib. Mineral. Petrol. 149 (1), 57–84. https://doi.org/10.1007/s00410-004-0635-6.

Kendrick, J., Yakymchuk, C., 2020. Garnet fractionation, progressive melt loss and bulk composition variations in anatectic metabasites: Complications for interpreting the geodynamic significance of TTGs. Geosci. Front. 11 (3), 745–763. https://doi.org/10.1016/j.gsf.2019.12.001.

Krogstad, E.J., Hanson, G.N., Rajamani, V., 1995. Sources of continental magmatism adjacent to the late Archean Kolar Suture Zone, south India: Distinct isotopic and elemental signatures of two late Archean magmatic series. Contrib. Mineral. Petrol. 122 (1-2), 159–173. https://doi.org/10.1007/s004100050119.

Król, P., Kusiak, M.A., Dunkley, D.J., Wilde, S.A., Yi, K., Lee, S., Kocjan, I., 2020. Diversity of Archean crust in the eastern Tula Mountains, Napier Complex, East Antarctica. Gondwana Res. 82, 151–170. https://doi.org/10.1016/j.gr.2019.12.014.

Kusiak, M.A., Dunkley, D.J., Wilde, S.A., Whitehouse, M.J., Kemp, A.I.S., 2021. Eoarchean crust in East Antarctica: Extension from Enderby Land into Kemp Land. Gondwana Res. 93, 227–241. https://doi.org/10.1016/j.gr.2020.12.031.

Kusiak, M.A., Whitehouse, M.J., Wilde, S.A., Dunkley, D.J., Menneken, M., Nemchin, A.A., Clark, C., 2013a. Changes in zircon chemistry during archean UHT metamorphism in the Napier Complex, Antarctica. Am. J. Sci. 313 (9), 933–967. https://doi.org/10.2475/09.2013.05.

Kusiak, M.A., Whitehouse, M.J., Wilde, S.A., Nemchin, A.A., Clark, C., 2013b. Mobilization of radiogenic Pb in zircon revealed by ion imaging: Implications for early Earth geochronology. Geology 41 (3), 291–294. https://doi.org/10.1130/G33920.110.1130/2013099.

Laurent, O., Martin, H., Moyen, J.-F., Doucelance, R., 2014. The diversity and evolution of late-Archean granitoids: Evidence for the onset of "modern-style" plate tectonics between 3.0 and 2.5 Ga. Lithos 205, 208–235. https://doi.org/10.1016/j.lithos.2014.06.012.

Ludwig, K.R., 2009. SQUID II User's Manual. Berkeley Geochronol. Cent. Spec. Publ. 100.

Ludwig, K.R., 2012. Isoplot 3.75, A Geochronological Toolkit for Microsoft Excel. Berkeley Geochronol. Cent. Spec. Publ. No. 5, 1–72. https://doi.org/10.1038/s41598-018-24631-5.

Lyon, I.C., Kusiak, M.A., Wirth, R., Whitehouse, M.J., Dunkley, D.J., Wilde, S.A., Schaumlöffel, D., Malherbe, J., Moore, K.L., 2019. Pb nanospheres in ancient zircon yield model ages for zircon formation and Pb mobilization. Sci. Rep. 9, 1–9. https://doi.org/10.1038/s41598-019-49882-8.

Marchildon, N., Brown, M., 2003. Spatial distribution of melt-bearing structures in anatectic rocks from Southern Brittany, France: Implications for melt transfer at grain- to orogen-scale. Tectonophysics 364 (3-4), 215–235. https://doi.org/10.1016/S0040-1951(03)00061-1.

Martin, H., Smithies, R.H., Rapp, R., Moyen, J.F., Champion, D., 2005. An overview of adakite, tonalite-trondhjemiten-granodiorite (TTG), and sanukitoid: Relationships and some implications for crustal evolution. Lithos 79, 1–24. https://doi.org/10.1016/j.lithos.2004.04.048.

McDonough, W.F., Sun, S.-S., 1995. The composition of the earth. Chem. Geol. 67, 1050–1056.

Middlemost, E.A.K., 1994. Naming materials in the magma/igneous rock system. Earth Sci. Rev. 37 (3-4), 215–224. https://doi.org/10.1016/0012-8252(94)90029-9.

Mitchell, R.J., Harley, S.L., 2017. Zr-in-rutile resetting in aluminosilicate bearing ultra-high temperature granulites: Refining the record of cooling and hydration in the Napier Complex, Antarctica. Lithos 272–273, 128–146. https://doi.org/10.1016/j.lithos.2016.11.027.

Mohan, M.R., Asokan, A.D., Wilde, S.A., 2020. Crustal growth of the Eastern Dharwar Craton: A Neoarchean collisional orogeny? Geol. Soc. Spec. Publ. 489 (1), 51–77. https://doi.org/10.1144/SP489-2019-108.

Mohan, M.R., Piercey, S.J., Kamber, B.S., Sarma, D.S., 2013. Subduction related tectonic evolution of the Neoarchean eastern Dharwar Craton, southern India: New geochemical and isotopic constraints. Precambr. Res. 227, 204–226. https://doi.org/10.1016/j.precamres.2012.06.012.

Moyen, J.-F., 2011. The composite Archaean grey gneisses: Petrological significance, and evidence for a non-unique tectonic setting for Archaean crustal growth. Lithos 123 (1-4), 21–36. https://doi.org/10.1016/j.lithos.2010.09.015.

Moyen, J.-F., 2019. Archean granitoids: classification, petrology, geochemistry and origin. Geol. Soc. London Spec. Publ. 489 (1), 15–49. https://doi.org/10.1144/SP489-2018-34.

Moyen, J.-F., Champion, D., Smithies, R.H., 2009. The geochemistry of Archaean plagioclase-rich granites as a marker of source enrichment and depth of melting. Earth Environ. Sci. Trans. R. Soc. Edinburgh 100 (1-2), 35–50. https://doi.org/10.1017/S1755691009016132.

Moyen, J.-F., Jayananda, M., Nédélec, A., Martin, H., Mahabaleswar, B., Auvray, B., 2003. From the roots to the roof of a granite: The Closepet Granite of south India. J. Geol. Soc. India 62, 753–768.

Moyen, J.-F., Martin, H., 2012. Forty years of TTG research. Lithos 148, 312–336. https://doi.org/10.1016/j.lithos.2012.06.010.

Moyen, J.-F., Martin, H., Jayananda, M., 2001. Multi-element geochemical modelling of crust-mantle interactions during late-Archaean crustal growth: The Closepet granite (South India). Precambr. Res. 112 (1-2), 87–105. https://doi.org/10.1016/S0301-9268(01)00171-1.

Moyen, J.-F., Laurent, O., 2018. Archaean tectonic systems: A view from igneous rocks. Lithos 302–303, 99–125. https://doi.org/10.1016/j.lithos.2017.11.038.

Moyen, J.-F., Stevens, G., 2006. Experimental constraints on TTG petrogenesis: Implications for Archean geodynamics. In: Benn, K., Mareschal, J.-C., Condie, K.C. (Eds.), Archean Geodynamics and Environments. Blackwell Publishing Ltd, pp. 149–175. https://doi.org/10.1029/164GM11.

O'Connor, J.T., 1965. A classification for quartz-rich igneous rocks. US Geological Survey Prof. Pap. 525, 79.

Owada, M., Osanai, Y., Kagami, H., 1994. Isotopic equilibration age of Sm-Nd whole-rock system in the Napier Complex (Tonagh Island), East Antarctica. Proc. NIPR Symp. Antarct. Geosci. 7, 122–132.

Paces, J.B., Miller, J.D., 1993. Precise U-Pb ages of Duluth complex and related mafic intrusions, northeastern Minnesota: Geochronological insights to physical, petrogenetic, paleomagnetic, and tectonomagmatic processes associated with the 1.1 Ga midcontinent rift system. J. Geophys. Res. Solid Earth 98 (B8), 13997–14013. https://doi.org/10.1029/93JB01159.

Palin, R.M., White, R.W., Green, E.C.R., Diener, J.F.A., Powell, R., Holland, T.J.B., 2016. High-grade metamorphism and partial melting of basic and intermediate rocks. J. Metam. Geol. 34 (9), 871–892. https://doi.org/10.1111/jmg.12212.

Pourteau, A., Doucet, L.S., Blereau, E.R., Volante, S., Johnson, T.E., Collins, W.J., Li, Z.-X., Champion, D.C., 2020. TTG generation by fluid-fluxed crustal melting: Direct evidence from the Proterozoic Georgetown Inlier, NE Australia. Earth Planet. Sci. Lett. 550, 116548. https://doi.org/10.1016/j.epsl.2020.116548.

Prabhakar, B.C., Jayananda, M., Shareef, M., Kano, T., 2009. Petrology and geochemistry of late Archaean granitoids in the northern part of Eastern Dharwar Craton, Southern India: Implications for transitional geodynamic setting. J. Geol. Soc. India 74 (3), 299–317. https://doi.org/10.1007/s12594-009-0137-2.

Rapp, R.P., Watson, E.B., Miller, C.F., 1991. Partial melting of amphibolite/eclogite and the origin of Archean trondhjemites and tonalites. Precambr. Res. 51 (1-4), 1–25. https://doi.org/10.1016/0301-9268(91)90092-O.

Rubatto, D., 2017. Zircon: The Metamorphic Mineral. Rev. Mineral. Geochem. 83, 261–295. https://doi.org/10.2138/rmg.2017.83.9.

Santosh, M., Wilde, S., Li, J., 2007. Timing of Paleoproterozoic ultrahigh-temperature metamorphism in the North China Craton: Evidence from SHRIMP U-Pb zircon geochronology. Precambr. Res. 159 (3-4), 178–196. https://doi.org/10.1016/j.precamres.2007.06.006.

Sarvothaman, H., 2001. Archean high-Mg granitoids of mantle origin in the Eastern Dharwar Craton of Andhra Pradesh. J. Geol. Soc. India 58, 261–268.

Schaltegger, U., Davies, J.H.F.L., 2017. Petrochronology of Zicon and Baddeleyite in Igneous Rocks: Reconstructing Magmatic Processes at High Temporal Resolution. Rev. Min. Geochem. 83, 297–328. https://doi.org/10.2138/rmg.2017.83.10.

Sheraton, J.W., Black, L.P., 1983. Geochemistry of Precambrian gneisses: relevance for the evolution of the East Antarctic Shield. Lithos 16 (4), 273–296.

Sheraton, J.W., Ellis, D.J., Kuehner, S.M., 1985. Rare-Earth Element Geochemistry of Archean Orthogneisses and Evolution of the East Antarctic Shield. BMR J. Aust. Geol. Geophys. 9, 207–218.

Sheraton, J.W., Tingey, R.J., Black, L.P., Offe, L.A., Ellis, D.J., 1987. Geology of Enderby Land and western Kemp Land, Antarctica. Bur. Miner. Resour. Geol. Geophys. Bull. 223, 1–51.

Shiraishi, K., Dunkley, D.J., Hokada, T., Fanning, C.M., Kagami, H., Hamamoto, T., 2008. Geochronological constraints on the Late Proterozoic to Cambrian crustal evolution of eastern Dronning Maud Land, East Antarctica: a synthesis of SHRIMP U-Pb age and Nd model age data. Geol. Soc. Lond. Spec. Publ. 308 (1), 21–67. https://doi.org/10.1144/SP308.2.

Smithies, R.H., Lu, Y., Johnson, T.E., Kirkland, C.L., Cassidy, K.F., Champion, D.C., Mole, D.R., Zibra, I., Gessner, K., Sapkota, J., De Paoli, M.C., Poujol, M., 2019. No evidence for high-pressure melting of Earth's crust in the Archean. Nat. Commun. 10, 1–12. https://doi.org/10.1038/s41467-019-13547-x.

Sobotovich, E.V., Kamenev, V.N., Kornanstyy, A.A., Rudnik, V.A., 1976. The oldest rocks of Antarctica (Enderby Land). Int. Geol. Rev. 18 (4), 371–388. https://doi.org/10.1080/00206817609471218.

Stacey, J.S., Kramers, J.D., 1975. Approximation of terrestrial lead isotope evolution by a two-stage model. Earth Planet. Sci. Lett. 26 (2), 207–221. https://doi.org/10.1016/0012-821X(75)90088-6.

Suzuki, S., Arima, M., Williams, I., Shiraishi, K., Kagami, H., 2006. Thermal History of UHT Metamorphism in the Napier Complex, East Antarctica: Insights from Zircon, Monazite, and Garnet Ages. J. Geol. 114 (1), 65–84. https://doi.org/10.1086/498100.

Takehara, M., Horie, K., Hokada, T., 2020. Geochemical characterization of zircon in Fyfe Hills of the Napier Complex, East Antarctica. Minerals 10, 1–15. https://doi.org/10.3390/min10110943.

Waters, D.J., 1988. Partial melting and the formation of granulite facies assemblages in Namaqualand, South Africa. J. Metam. Geol. 6 (4), 387–404. https://doi.org/10.1111/j.1525-1314.1988.tb00430.x.

Wiedenbeck, M., Alle, P., Corfu, F., Griffin, W.L., Meier, M., Oberli, F., von Quadt, A., Roddick, J.C., Spiegel, W., 1995. Three natural zircon standards for U-Th-Pb, Lu-Hf, trace element and REE analyses. Geostand. Newsl. 19, 1–23. https://doi.org/10.1111/j.1751-908X.1995.tb00147.x.

White, R.W., Palin, R.M., Green, E.C.R., 2017. High-grade metamorphism and partial melting in Archean composite grey gneiss complexes. J. Metam. Geol. 35 (2), 181–195. https://doi.org/10.1111/jmg.12227.

White, R.W., Powell, R., 2002. Melt loss and the preservation of granulite facies mineral assemblages. J. Metam. Geol. 20, 621–632. https://doi.org/10.1046/j.1525-1314.2002.00206_20_7.x.

Williams, I.S., 1998. U-Th-Pb Geochronology by Ion Microprobe. In: McKibben, M.A., Shanks III, W.C., Ridley, W.I. (Eds.). Applications of Microanalytical Techniques to Understanding Mineralizing Processes, vol. 7, Reviews in Economic Geology, pp. 1–35.

Yakymchuk, C., Kirkland, C.L., Clark, C., 2018. Th/U ratios in metamorphic zircon. J. Metamorph. Geol. 36 (6), 715–737. https://doi.org/10.1111/jmg.12307.

Zachariah, J.K., Rajamani, V., Hanson, G.N., 1997. Petrogenesis and source characteristics of metatholeiites from the Archean Ramagiri schist belt, eastern part of Dharwar craton. India. Contrib. to Mineral. Petrol. 129, 87–104. https://doi.org/10.1007/s004100050325.